

Principal Hugoniot, reverberating wave, and mechanical reshock measurements of liquid deuterium to 400 GPa using plate impact techniques

M. D. Knudson, D. L. Hanson, J. E. Bailey, C. A. Hall, J. R. Asay,* and C. Deeney
Sandia National Laboratories, Albuquerque, New Mexico 87185-1181, USA

(Received 8 October 2003; revised manuscript received 13 January 2004; published 29 April 2004)

The high-pressure response of cryogenic liquid deuterium (LD_2) has been studied to pressures of ~ 400 GPa and densities of ~ 1.5 g/cm³. Using intense magnetic pressure produced by the Sandia National Laboratories Z accelerator, macroscopic aluminum or titanium flyer plates, several mm in lateral dimensions and a few hundred microns in thickness, have been launched to velocities in excess of 22 km/s, producing constant pressure drive times of approximately 30 ns in plate impact, shock wave experiments. This flyer plate technique was used to perform shock wave experiments on LD_2 to examine its high-pressure equation of state. Using an impedance matching method, Hugoniot measurements of LD_2 were obtained in the pressure range of ~ 22 –100 GPa. Results of these experiments indicate a peak compression ratio of approximately 4.3 on the Hugoniot. In contrast, previously reported Hugoniot states inferred from laser-driven experiments indicate a peak compression ratio of approximately 5.5–6 in this same pressure range. The stiff Hugoniot response observed in the present impedance matching experiments was confirmed in simultaneous, independent measurements of the relative transit times of shock waves reverberating within the sample cell, between the front aluminum drive plate and the rear sapphire window. The relative timing was found to be sensitive to the density compression along the principal Hugoniot. Finally, mechanical reshock measurements of LD_2 using sapphire, aluminum, and α -quartz anvils were made. These results also indicate a stiff response, in agreement with the Hugoniot and reverberating wave measurements. Using simple model-independent arguments based on wave propagation, the principal Hugoniot, reverberating wave, and sapphire anvil reshock measurements are shown to be internally self-consistent, making a strong case for a Hugoniot response with a maximum compression ratio of ~ 4.3 –4.5. The trends observed in the present data are in very good agreement with several *ab initio* models and a recent chemical picture model for LD_2 , but in disagreement with previously reported laser-driven shock results. Due to this disagreement, significant emphasis is placed on the discussion of uncertainties, and the potential systematic errors associated with each measurement.

DOI: 10.1103/PhysRevB.69.144209

PACS number(s): 64.30.+t, 62.50.+p

I. INTRODUCTION

The past several years have seen a significant interest in the high-pressure response of hydrogen and its isotopes. This is primarily due to the unexpected dynamic response of liquid deuterium (LD_2) inferred from laser-driven experiments by Da Silva *et al.*¹ and Collins *et al.*² In their work, it was reported that the maximum shock compression of LD_2 along the principal Hugoniot exceeds sixfold, which is significantly higher than the \sim fourfold maximum shock compression predicted by the widely used and accepted theoretical models at the time.^{3–5} This increase in limiting shock compression, if legitimate, would have significant impact across a broad scientific spectrum; it would influence capsule design for inertial confinement fusion (ICF) studies, it would alter our fundamental understanding of the formation of the giant planets, and it would also question our theoretical understanding of the most prominent, and simplest, element in the universe. Since these initial reports, hydrogen and deuterium have been the focus of numerous experimental and theoretical studies in an attempt to explain this apparent anomaly.

As of this writing, there is yet no clear answer to this discrepancy in the high-pressure response of hydrogen. After the initial publications from Da Silva *et al.*¹ and Collins *et al.*,² Mostovych *et al.* reported an independent confirmation of the enhanced compression based on a mechanical

reshock technique in laser-driven experiments.^{6,7} Shortly thereafter, our group at Sandia National Laboratories (SNL) reported experimental results using a plate-impact impedance matching technique that are inconsistent with the laser-driven results; rather, our results indicate a maximum compression along the principal Hugoniot of ~ 4.3 -fold.⁸ Later, we reported an independent confirmation of our Hugoniot results based on a reverberating wave technique.⁹ Finally, more recent results from Russian investigators, obtained using a convergent geometry technique to achieve shock pressures up to ~ 100 GPa,^{10–12} agree with the stiffer Hugoniot response reported by our group. Meanwhile, experimental efforts are continuing at the Omega laser facility at the University of Rochester to obtain reshock and impedance matching Hugoniot data using laser driven shock wave loading.¹³

We also note that in a recent publication Nellis¹⁴ critically examined the differences between the laser-driven^{1,2} and magnetically driven flyer plate results.⁸ He argued that the stiffer Hugoniot response is expected for LD_2 , based on the universal behavior of other low- Z diatomic liquids undergoing single-shock compression and molecular dissociation.

On the theoretical front, publications have come out in support of both the stiff and soft Hugoniot response. Notably, nearly all of the first principles *ab initio* based models seem to be converging toward a stiff response at high pressures. Recent publications describing path-integral Monte Carlo

(PIMC)^{15,16} and several variations of finite temperature (FT) density functional theory (DFT) (Refs. 17–23) show consistency with a stiff Hugoniot response, in relatively good agreement with the SNL and Russian results, as well as the earlier chemical picture models.^{3–5} The one exception is the results of Gygi and Galli²⁴ where a Car-Parrinello technique was used in a quantum molecular dynamics (QMD) simulation of shock wave propagation through a LD_2 sample. Enhanced compressions, along with departures from the Born-Oppenheimer surface, were observed for large values of the artificial fictitious mass, a free parameter used to accelerate convergence in equilibrium Car-Parrinello simulations. This led to the suggestion that nonequilibrium effects could have influenced the observations of the laser groups. It should be noted that this result is somewhat controversial given that no physical picture has been presented to relate these departures from the Born-Oppenheimer surface to actual nonadiabatic effects. To the best of our knowledge the only other models for LD_2 that exhibit such a soft response, commensurate with the laser-driven results, are a few of the chemical picture models.^{25–30}

The persistence of this discrepancy is largely due to the difficulty of the experiments. In particular, the relevant pressure levels are sufficiently high, above the pressures attainable through explosively driven³¹ or gas gun techniques,^{32–34} that only a few facilities in the world can address this issue experimentally. These include large lasers facilities, the Z accelerator, and spherically convergent high explosive systems in Russia. Furthermore, the high shock compression of LD_2 requires that experimental observables be measured with extreme accuracy—a requirement that is difficult to achieve, given the sample sizes in these experiments are typically small in order to reach the necessary energy densities. These experimental difficulties complicate an accurate determination of density compression using traditional Hugoniot pressure-density measurements, and have led to the development of complementary measurement techniques in an attempt to discern the limiting shock compression of LD_2 . Examples of these techniques are the reshock technique, first implemented by Mostovych *et al.*,^{6,7} and the recently developed reverberating wave technique, first implemented by our group.^{9,35,36} However, direct comparisons of results from the different techniques is difficult because, with few exceptions, these various techniques have not previously been performed on the same experimental platform.

As a step towards remedying this situation, in this paper we discuss a comprehensive study of the high-pressure mechanical response of LD_2 , using a plate-impact technique developed at the Sandia Z accelerator. A combination of traditional impedance matching Hugoniot measurements, reverberating wave measurements, and reshock measurements have been made over a pressure range of ~ 20 –400 GPa. In the most recent experiments, these measurements were obtained not only on the same experimental platform, but during the same experiment, thus enabling detailed comparisons and consistency checks to be made. The results of these various measurements are shown to be internally self-consistent, and further support the conclusion that LD_2 exhibits a maximum compression of ~ 4.3 –4.5 on the Hugoniot, in good

agreement with most *ab initio* models and the chemical picture models that predict a stiff Hugoniot response. In particular, the results reported here are shown to be in exceptional agreement with a recent FT-DFT model by Desjarlais²³ and a recent complete revision of the Sesame 72 chemical picture model by Kerley, which will be referred to as the “Kerley 03” model.^{37,38}

Section II provides a description of the experimental method used to perform the high-pressure study of LD_2 . Experimental results for each of the three experimental techniques are separately discussed in Sec. III. Section IV provides a summary of results for the high-pressure response of LD_2 , with an emphasis on the observed internal consistency between the methods. Detailed discussions regarding uncertainties and potential systematic errors associated with the measurements are given in Sec. V and in the Appendix. The main conclusions are summarized in Sec. VI.

II. EXPERIMENTAL TECHNIQUE

Dynamic high-pressure experiments were performed on planar LD_2 samples using flyer plate impact techniques developed at the Sandia Z accelerator.³⁹ The flyer plates comprise the anode of the short-circuit load at the center of the Z accelerator (see Figs. 1 in Ref. 41). The interaction of the current density and magnetic field produced in the insulating gap results in a time-dependent pressure history $P(t)$ that is applied to the inner surface of the flyer plate. In the present experiments, $P(t)$ increases approximately linearly over a ~ 200 ns rise time, resulting in an impulsive ramp load that provides momentum to the anode, launching it as an effective flyer plate to a prescribed velocity.

Typically, four aluminum anode panels are arranged about a central, square, or rectangular stainless steel cathode post, forming a symmetric anode-cathode gap (A - K gap). A short circuit is created between the anode panels and cathode post through a shorting cap at the top of the coaxial load. Each anode panel becomes a flyer plate; this is achieved by machining the entire current carrying portion of the aluminum anode panel to a prescribed thickness of 800–900 μm . To retain rigidity, and to allow the panels to be assembled together, the flyer frame is attached to a panel back (see Fig. 1 in Ref. 41). The panel back also allows for mounting of the experimental target at a prescribed distance from the flyer plate, which is typically ~ 3 –4 mm. An alternate configuration employs a thinner aluminum plate that acts as a driver to launch a separate, embedded titanium flyer. The current carrying surface of each panel and the impact surface of the flyer are flat to ~ 200 nm and parallel to ~ 2 μm with ~ 20 nm surface finishes. Each panel back can hold two separate targets, allowing up to eight simultaneous shock wave experiments during a single firing of the accelerator.

The square geometry produces a peak magnetic pressure of ~ 100 GPa, which is capable of launching aluminum flyers up to a maximum velocity of ~ 16 km/s and titanium flyers up to a maximum velocity of ~ 14 km/s. The rectangular or slab geometry, which increases the current density at the expense of two flyer plates, produces a peak magnetic pressure of ~ 250 GPa, which is capable of launching alumi-

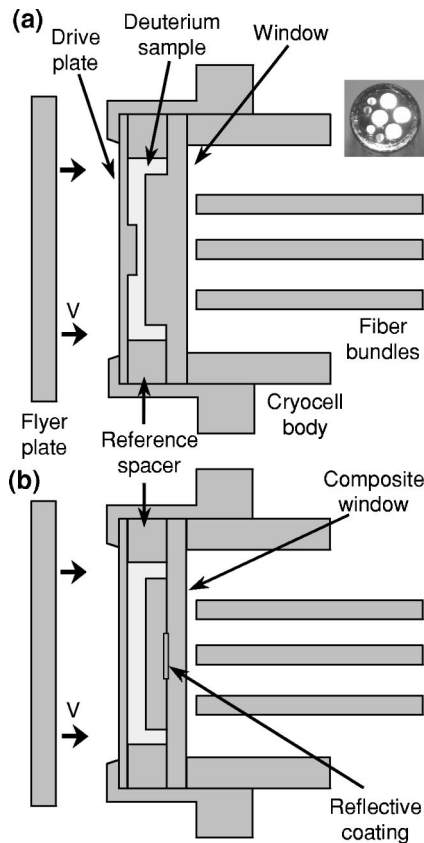


FIG. 1. Experimental configuration used to obtain EOS data for LD_2 . (a) Hugoniot and reverberating wave measurements and (b) Hugoniot, reverberating wave, and reshock measurements. Note the drawing is not to scale. Inset shows fiber arrangement in each fiber bundle.

num flyers up to a maximum velocity of ~ 25 km/s and titanium flyers up to a maximum velocity of ~ 22 km/s. Further details concerning the launch of the flyer plate and the quality of the resulting impact can be found in Refs. 40–43.

The necessary cryogenic capability was provided by an expendable cryocell containing the LD_2 sample, which was connected to a survivable cryostat.⁴⁴ The cryocell consisted of an aluminum drive plate and an optically transparent window housed within an OFHC copper body. The cell dimensions were determined with copper reference spacers, the dimensions of which were measured prior to assembly using interferometric techniques, accurate to $\sim 1 \mu\text{m}$. The dimensions of the LD_2 cell at cryogenic temperatures were determined from the interferometric measurements and the known thermal expansions of the cell materials.^{45,46} The uncertainty in the linear thermal expansion correction at all temperatures for all of the materials is small, typically $\sim 3\%$, so the uncertainty in the original length measurement at room temperature dominates.⁴⁷ The final accuracy in the cell dimensions was better than 1%.

Two types of LD_2 sample cells were used, shown schematically in Figs. 1(a) and 1(b). Initial experiments used a stepped aluminum drive plate, with nominal thicknesses of 200 and 500 μm . This produced LD_2 samples with dimensions of ~ 600 and $\sim 300 \mu\text{m}$ in thickness and ~ 5 mm in

diameter. In these experiments the stepped drive plate was utilized in order to obtain additional data regarding the shocked state of the aluminum. In later experiments the stepped drive plates were replaced by flat aluminum drive plates of $\sim 250 \mu\text{m}$ thickness. This was done in order to obtain other experimental data in addition to the principal Hugoniot; in particular reshock measurements required a flat drive plate in order to minimize side perturbations. These later experiments also utilized a modified back window, which will be referred to as a composite window. The back portion of the composite window, which made the seal with the cryocell body, was a sapphire window of $\sim 500 \mu\text{m}$ thickness. The front portion of the composite window, in contact with the LD_2 , consisted of a $\sim 250 \mu\text{m}$ thick bonded plate of sapphire, α quartz, or a combination of LiF and aluminum [see Fig. 1(b)]. In each case, the central portion of the window provided a reflective surface at the interface between the front and back window materials. This was either an aluminized coating on the sapphire or α quartz, or the aluminum sample itself. Adjacent to the reflective surface there was diagnostic access into the cell. This was provided either by LiF samples of similar thickness to the aluminum, or by uncoated regions of the sapphire or α -quartz windows. In these later experiments the LD_2 sample was $\sim 550 \mu\text{m}$ in thickness and ~ 5 mm in diameter.

The LD_2 samples were obtained by condensing high purity deuterium gas in the cryocell.⁴⁴ Prior to cooling, and after several filling and purging cycles to ensure trace atmospheric gases were not present, the cell was filled with high purity deuterium gas to 18 psi. The cell was then cooled to its equilibrium temperature of approximately 15 K. A resistive heater, controlled by a temperature sensor in a feedback loop, was used to heat the cell and maintain a temperature of $\sim 22.0 \pm 0.1$ K. This process produced a quiescent liquid sample below the boiling point of ~ 24.5 K, with a nominal initial density of 0.167 g/cm^3 . The typical uncertainty in initial density was $\sim 0.4\%$. The temperature of the cell was monitored via two silicon diode temperature sensors, one of which provided the feedback to the heater controller. Prior to the experiment on Z, each cell was tested in an off-line vacuum chamber to detect any leaks. During this test, the temperature of the cell was cycled through the boiling and melt temperatures of deuterium several times to calibrate the temperature sensors. Once in the Z accelerator, the cell was again cycled through the boiling and melt temperatures to verify the temperature calibration determined in the prior cooling test.

Planar shock waves were generated by impact of either an aluminum (6061-T6) or titanium (Ti-Al6V4) flyer plate onto the aluminum drive plate at the front of the cell. The rectangular flyer plate, approximately 12×25 mm in lateral dimension by $\sim 300 \mu\text{m}$ in effective thickness,^{40–43,48} was accelerated across a nominal 3–4 mm vacuum gap by the magnetic field. Titanium flyer velocities in excess of 22 km/s were achieved, capable of generating shock states to ~ 700 GPa in the aluminum drive plate and transmitting up to ~ 100 GPa shock waves into the LD_2 sample. The flyer plate velocity was directly measured using conventional velocity interferometry⁴⁹ (VISAR, velocity interferometer system for

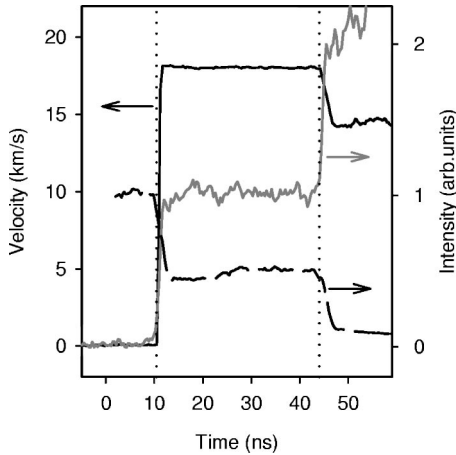


FIG. 2. Typical data obtained in a LD_2 experiment, in this case Z824S; (i) VISAR record of the shock front (solid black line), (ii) FOSBO record (dashed black line), and (iii) self-emission record (gray line). Vertical dotted lines indicate break out of the shock from the aluminum/ LD_2 interface and the arrival of the shock at the LD_2 /window interface.

any reflector) to a typical accuracy of $\sim 0.5\text{--}1\%$. However, in some cases the quality of the VISAR signal resulted in a somewhat lower accuracy of $\sim 2\text{--}3\%$. The velocity was measured using multiple VISAR probes at a point adjacent to the LD_2 cell. Details can be found in Ref. 41.

The shock response of LD_2 was diagnosed with several different fiber-optic coupled diagnostics. The relatively large samples in these experiments enabled several optical fiber bundles of 100 and 200 μm diameter fibers to be used. These fiber bundles accessed different lateral positions of the sample, allowing the fielding of multiple, redundant diagnostics. These included (i) conventional VISAR, (ii) fiber-optic shock break out (FOSBO), and (iii) spectrally and temporally resolved spectroscopy. The fringe data from the conventional VISAR diagnostic, which in these experiments is indicative of the Doppler shift from the shock front of the LD_2 (at shock pressures above ~ 30 GPa LD_2 becomes reflective²), was recorded on a digitizer at a sampling rate of either 4 or 5 Gigasample/s. However, the VISAR diagnostic used photomultiplier tubes (PMT) to convert the light signal to an electrical signal, thus the time resolution of VISAR data was limited to $\sim 1\text{--}2$ ns. The FOSBO diagnostic, sensitive to the sudden change in reflectivity upon emergence of a strong shock, utilized a streak camera to provide high time-resolution recording of the reflected signal. Typically, the streak rate of the FOSBO camera was set to provide $\sim 50\text{--}200$ ns of recording time, resulting in a temporal resolution of $\sim 0.25\text{--}1$ ns. The spectrally and temporally resolved spectroscopy diagnostic utilized a spectrometer to provide wavelength dispersion, and a streak camera to provide temporal resolution. Typically, the streak rate of the spectroscopy camera was set to provide $\sim 100\text{--}200$ ns of recording time, resulting in a temporal resolution of $\sim 0.5\text{--}1$ ns.

Figure 2 shows sample data obtained from a typical LD_2 experiment (experiment Z824S).⁵⁰ Sixteen channels of data from VISAR, FOSBO, and self-emission fibers were ob-

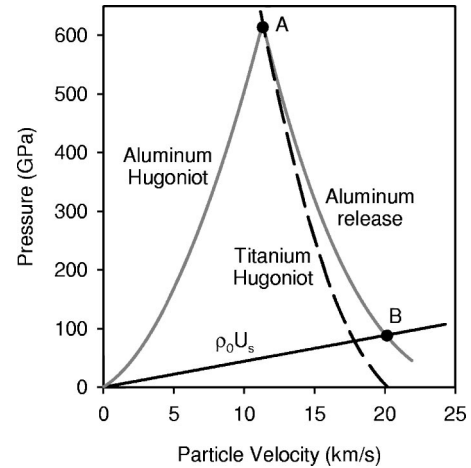


FIG. 3. Impedance matching method used to obtain u_p for LD_2 .

tained for each experiment, allowing up to 16 independent measurements of the shock velocity in the LD_2 sample. In experiments with a stepped aluminum drive plate, up to four independent measurements of the shock velocity in the aluminum drive plate were obtained. Likewise, in the experiments with a composite window, 2–6 independent measurements of the shock velocity in the anvil material were obtained. These multiple, redundant measurements allowed the use of statistical techniques to decrease uncertainty in the measured velocities,⁵¹ with typical uncertainties of $\sim 0.5\text{--}2$, ~ 3 , and $\sim 1.5\text{--}3\%$ in the measured LD_2 , drive plate, and anvil shock velocities, respectively. In addition to shock velocities in the LD_2 sample, drive plate, and anvil material, accurate measurements of the reverberation timing, and the spectral dispersion of self-emission from the shocked LD_2 were obtained. Analysis of all mechanical measurements will be discussed in the next sections. Detailed analysis of the spectral dispersion of the self-emission, which provides a measure of the temperature of the shocked LD_2 , can be seen in Ref. 52, and was found to be completely consistent with the mechanical measurements described herein.

A. Principal Hugoniot experiments

The impedance matching method, utilizing the Hugoniot jump conditions,⁵³ was used to obtain principal Hugoniot data for the shocked LD_2 . The shocked state of the drive plate was determined using the known equation of state (EOS) of the flyer plate (aluminum or titanium) and drive plate (aluminum), and the measured flyer velocity u_v . A graphical representation of the impedance matching method is shown in Fig. 3. The initial shocked state of the aluminum drive plate is described in the pressure-particle velocity (P - u_p) plane by the point labeled A, which corresponds to the intersection of the aluminum drive plate Hugoniot, centered at $P=0, u_p=0$, and the flyer plate Hugoniot, in this case titanium, centered at $P=0, u_p=u_v$. Since $P = \rho_0 U_s u_p$, the shocked state of the LD_2 is constrained to lie on a straight line of slope $\rho_0 U_s$, where ρ_0 is the initial density of the LD_2 sample and U_s is the measured shock

velocity. u_p of the LD_2 is determined by the intersection of the aluminum release isentrope from state A and the line defined by the shock impedance of LD_2 , indicated by point B in Fig. 3. In the present study the Sesame 3700 EOS model for aluminum⁵⁴ was used to calculate the release isentrope from state A in the aluminum drive plate. We note that in using a calculated release curve, there is a potential for systematic error in the inferred u_p ; this issue will be addressed in detail in Sec. V. Given u_p , the density compression is then determined from the momentum conservation equation using the expression $\rho_1/\rho_0 = U_s/(U_s - u_p)$. The uncertainty in the inferred u_p for LD_2 determined in this way was typically $\sim 2-4\%$. Details concerning the uncertainty analysis can be seen in the Appendix.

In several cases, the driving pressure pulse used to launch the flyer plate formed a small shock prior to reaching the free surface of the flyer (impact side). This was evident by a sudden jump in the flyer velocity upon initial motion to u_j , referred to as the jump-off velocity (see Ref. 41). Dissipative processes associated with this initial shock compression result in a slightly elevated temperature of the flyer plate, and thus a slightly lower density relative to the ambient state. This altered state of the flyer complicates the impedance matching analysis to determine the particle velocity state of the LD_2 . The method employed to compensate for this effect is the following. First, the measured u_j was used to determine the magnitude of the shock that formed in the flyer plate prior to the wave reaching the impact side of the flyer. An EOS model for aluminum (Sesame 3700)⁵⁴ or titanium (Sesame 4061)⁵⁵ was used to calculate the density ρ'_0 and temperature T'_0 , corresponding to an isentropic release from this shocked state; the thermodynamic state of the flyer at impact was assumed to be ρ'_0 and T'_0 .⁵⁶ The same aluminum or titanium EOS model was then used to calculate the modified Hugoniot for the flyer centered at ρ'_0 and T'_0 . This modified Hugoniot was then used in the impedance matching method described above to determine the shock state of the aluminum drive plate. This approach was previously validated in near-symmetric impact experiments to determine the Hugoniot of aluminum to ~ 500 GPa.⁴¹

It should also be mentioned that simultaneous with each experiment on LD_2 , a separate impact experiment was performed on a room temperature aluminum sample using the same flyer plate panel. Furthermore, the initial LD_2 experiments, which utilized stepped aluminum drive plates, provided a measure of the shock velocity in the aluminum drive plate. In both cases the shock velocity in the aluminum (either the ambient aluminum sample or the cryogenic drive plate) was determined from the FOSBO diagnostic to a typical accuracy of $\sim 3\%$. The measured shock velocity in aluminum was compared to the expected shock velocity inferred from the impedance matching method described above. In each case, agreement was observed between the two independent measurements, within experimental uncertainty. However, the state of the drive plate could be determined to a higher accuracy through impedance matching using the measured flyer velocity (typical uncertainty of $\sim 2-3\%$ in u_p) as opposed to the shock velocity measure-

ment ($\sim 3\%$ uncertainty in U_s translates to $\sim 5-6\%$ uncertainty in u_p). Consequently, impedance matching was the preferred method used to infer the shock state of the aluminum drive plate in these experiments (see the Appendix for details).

B. Reverberating wave experiments

In typical shock wave experiments, the shock velocity U_s and mass velocity u_p are measured, as for the Hugoniot experiments described above. Conservation of mass and momentum are then used (the Rankine-Hugoniot jump conditions⁵³) to determine pressure $P = \rho_0 U_s u_p$ and density compression $\rho_1/\rho_0 = U_s/(U_s - u_p)$. However, uncertainties in U_s and u_p are magnified when converting to the density plane; specifically, the fractional errors in U_s and u_p are multiplied by the factor $(\rho_1/\rho_0 - 1)$ (approximately 3–3.5 for LD_2). Thus, for highly compressible materials such as LD_2 , in which u_p approaches U_s , moderate uncertainties in U_s and u_p lead to significant uncertainties in the inferred density compression.

A previous publication⁹ described the use of a reverberating wave technique to infer density compression along the principal Hugoniot. The technique involves monitoring the relative arrival time of shock waves at the LD_2 /sapphire interface as the shock reverberates between the aluminum drive plate and the sapphire window. This relative timing, which we will show is related to the density compression, can be used to distinguish between different density values for LD_2 in this higher pressure regime. Further, since the uncertainty in this measurement is not as sensitive to the magnitude of the density compression, it is particularly well suited for use with highly compressible materials, such as LD_2 .

After the shock initially traverses the cell, wave interactions at the LD_2 /sapphire interface result in a transmitted and a reflected shock, as shown in Fig. 4. This is exploited by using the reflected shock to probe the location of the aluminum/ LD_2 interface. The relative velocities of the initial shock (U_{s1}) and the aluminum/ LD_2 interface (u_{p1}) are directly related to the density compression along the Hugoniot. The velocities of the shock and the aluminum/ LD_2 interface determine the time that the reflected shock from the aluminum/ LD_2 interface reaches the LD_2 /sapphire interface. Thus, the ratio of the original transit time across the LD_2 cell ($t_1 - t_0$) to the time between the first and second shock arrival at the LD_2 /sapphire interface ($t_2 - t_1$), which will be referred to as the reverberation ratio, is related to the density compression of the LD_2 in the Hugoniot state.

Qualitatively, one can see from the position-time plot in Fig. 4 (drawn to scale for an initial shock of ~ 45 GPa in LD_2) that due to the substantial compression of LD_2 upon first shock, the exact behavior of LD_2 upon reshock has a relatively small influence on the reverberation ratio. The comparatively short reverberation time ($t_2 - t_1$) observed is directly related to the large density compression along the principal Hugoniot. Furthermore, since the reverberation ratio is obtained from a self-emission measurement on a single streak camera image, it can be determined to a high degree of

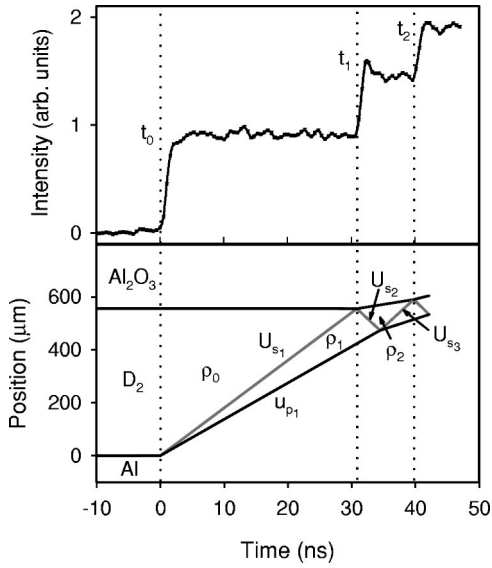


FIG. 4. Top: Typical self-emission measurement indicating shock arrival at the aluminum/ LD_2 interface (t_0), the first shock arrival at the LD_2 /sapphire interface (t_1), and the second shock arrival at the LD_2 /sapphire interface (t_2). Bottom: Position-time diagram indicating trajectories of the shock fronts and interfaces.

accuracy, providing a particularly sensitive inference of the initial density compression of LD_2 .

One can show quantitatively the strong dependence of the reverberation ratio on ρ_1 . Analysis of the position-time plot reveals that the ratio of the original transit time t_i to the reverberation time t_r is given by

$$\frac{t_i}{t_r} \equiv \frac{(t_1 - t_0)}{(t_2 - t_1)} = \left[\rho_0 U_{s1} \left(\frac{1}{\rho_1 U_{s2}} + \frac{1}{\rho_2 U_{s3}} \right) \right]^{-1}, \quad (1)$$

where ρ_0 is the initial LD_2 density; ρ_1 and ρ_2 are the LD_2 densities due to the first and second shock, respectively; and U_{s1} , U_{s2} , and U_{s3} are the velocities of the first, second, and third shock, respectively. Equation (1) indicates that apart from the measured quantities ρ_0 and U_{s1} , the ratio t_i/t_r depends on ρ_1 , ρ_2 , U_{s2} , and U_{s3} . However, model predictions over the pressure range examined in this study indicate that to a very good approximation $\rho_2 \approx 1.9\rho_1$ (Ref. 57) and $U_{s3} \approx U_{s2} \approx 1.1U_{s1}$ for LD_2 ; Sesame 72,³ Kerley 03,³⁷ Young,³⁰ tight-binding (TB),¹⁹ generalized gradient approximation-molecular dynamics (GGA-MD),²⁰ and Desjarlais²³ model predictions were compared, and the variations from these relations were found to be less than 10% for each of the models. Given this similar behavior upon reshock for the various models being considered for LD_2 , one can show that to a good approximation $t_i/t_r \approx (\rho_1/\rho_0)/1.39 = 4.23\rho_1$, where ρ_1 is expressed in units of g/cm^3 . Thus, the reverberation ratio t_i/t_r is approximately proportional to the density compression along the Hugoniot. It is to be emphasized, however, that when comparing experimental measurements with the various models for LD_2 the above approximation is not needed since the models uniquely determine ρ_1 , ρ_2 , U_{s2} , and U_{s3} .

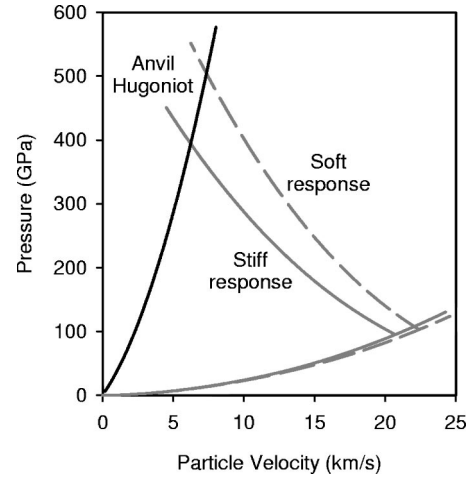


FIG. 5. Sensitivity of predicted reshock pressure to the EOS of LD_2 . Figure reconstructed from Ref. 7.

The reverberation time is obtained from time-resolved spectroscopy measurements; a typical spectroscopy measurement is shown in Fig. 4. The self-emission from the LD_2 sample provides a clear indication of shock arrival at the aluminum/ LD_2 interface (at time t_0) and also the first and second shock arrivals at the LD_2 /sapphire interface (at times t_1 and t_2 , respectively). In several cases these wave arrival times could also be clearly observed in the FOSBO measurement.⁵⁸ We emphasize that the experimental measurements reported here were possible due to the large sample sizes and long pressure drive times achievable with the flyer plate impact. The position-time plot shown in Fig. 4 demonstrates the need for constant pressures at the LD_2 /sapphire interface for times on order of ~ 30 – 40 ns in these experiments. The constancy of the emission signal during the initial transit time and the reverberation time indicates that the pressure remained constant through the full time duration of the experiment.⁵⁹

C. Reshock experiments

As mentioned above, the differences in observable quantities for the traditional Hugoniot experiment are small for LD_2 , forcing stringent requirements on the accuracy needed to distinguish between the various LD_2 models. Reverberating wave measurements are one alternative to identify differences in the predicted density compression, as discussed above. A second alternative measurement in this high pressure regime, which was employed by Mostovych *et al.*, is to measure the reshock state of LD_2 reflected from a known anvil material.^{6,7} As discussed by Mostovych, and shown in Fig. 5, the differences in predicted compression in the EOS models for deuterium are magnified after reshock from a high impedance anvil. For a given initial shock velocity in LD_2 , the softer EOS models predict a higher density, and therefore higher particle velocity, than do the stiffer models. The higher density and particle velocity result in higher predicted reshock pressures, and thus higher predicted shock velocities in the anvil material.

Mostovych *et al.* chose aluminum as the anvil due to the fact that aluminum is very well studied. In the present work,

emphasis was placed on sapphire as an anvil for two reasons. First, sapphire is transparent, and thus wave arrivals at various interfaces could be directly observed at the same lateral spatial position in the cell. This eliminates uncertainties due to nonplanar impacts that necessarily arise when inferring wave arrival through laterally separated measurements. Second, knowledge of the reshock state in LD_2 from a sapphire anvil provides additional information regarding the reverberating wave measurements described above. However, to compare with results obtained by Mostovych *et al.* (aluminum anvil)^{6,7} and recent measurements at the Omega laser facility (z -cut α -quartz anvil),¹³ both aluminum and α -quartz anvils were also used in the present study.

Shock velocity measurements in the anvil were made using both FOSBO and self-emission diagnostics. For the transparent anvils (sapphire and α quartz), composite windows such as the one shown schematically in Fig. 1(b) were used. A smaller diameter sapphire or α -quartz window was attached, using cryogenic epoxy on the edges of the anvil window, to a larger diameter sapphire window that comprised the back window of the cryocell. The central portion of the anvil window was coated with $\sim 1 \mu\text{m}$ of aluminum or silver, with the coated side in contact with the sapphire rear window. Fiber bundles were positioned directly behind the coated central region, allowing shock arrival time measurements at the anvil/sapphire interface to be determined, and on either side of the coated region, allowing shock arrival time at the LD_2 /anvil interface to be inferred. Furthermore, the probes on either side of the coated region also observed the arrival of the wave at the anvil/sapphire interface, which was apparent as a sudden change in the observed self-emission signal.

For the aluminum anvil experiments, a slightly different composite window was used. In this case, a small sample of aluminum ($\sim 2 \times 2 \text{ mm}$ square) was attached to the central region of the sapphire rear window, using cryogenic epoxy on the edges of the aluminum sample. On either side of the aluminum, similarly sized samples of LiF were attached to the sapphire, also using cryogenic epoxy on the edges. Probes were positioned directly behind the two LiF samples and the aluminum sample. The measured cell dimensions, the measured LD_2 shock velocity, and the measured shock arrival time at the LD_2 /LiF interface allowed the time at which the shock reached the LD_2 /aluminum interface to be inferred. The transit time in the aluminum anvil was then determined by comparing this inferred arrival time with the measured shock arrival time at the aluminum/sapphire interface.

In addition to the reshock measurements, principal Hugoniot measurements and reverberating wave measurements (for cells with sapphire anvils) were also made in the same experiment. To determine the appropriate thicknesses of the aluminum drive plate, LD_2 sample, and anvil material, while maximizing the transit times across the cell, and thus the accuracy of the Hugoniot and reverberating wave measurements, hydrodynamic simulations were performed using a 1D hydrocode CTH.⁶⁰ These simulations were necessary due to the numerous wave interactions at the various interfaces. Reverberation of the shock between the drive plate and anvil

material was of particular concern. Since the second shock in the anvil material, resulting from wave reverberation, has a Lagrangian wave speed that is significantly higher than that of the first shock, the second shock will overtake the first shock at some position in the anvil material. The inferred shock velocity in the anvil material would be slightly too high if this overtake occurred prior to the first shock fully traversing the anvil thickness.

Based on the hydrodynamic simulations nominal thicknesses of 250, 550, and 250 μm were chosen for the aluminum drive plate, LD_2 sample, and anvil material, respectively. For the lower pressure reshock experiments, these dimensions were sufficient to ensure that the second shock did not overtake the first shock within the anvil material. In these cases, the first shock velocity could be determined to an accuracy of $\sim 1.5\text{--}2\%$. However, for the higher pressure reshock experiments, the Lagrangian wave speed of the second shock proved to be high enough that the first shock was overtaken prior to reaching the anvil/sapphire interface; this is particularly true for the α -quartz anvil, which exhibits larger density compression upon first shock, and thus higher Lagrangian wave speeds. In these cases, the overtake within the anvil was observed in both the simulations and experiment; a few ns prior to the shock reaching the anvil/sapphire interface a significant increase in emission was observed in the self-emission measurements.⁶¹ In these cases, results from the hydrodynamic simulations were used to make a slight correction (of order 2%) to the first shock velocity in the anvil. With this correction, the first shock velocity could be determined to an accuracy of $\sim 3\%$.

III. EXPERIMENTAL RESULTS

A. Principal Hugoniot experiments

A total of 28 principal Hugoniot experiments were performed on LD_2 over a pressure range of $\sim 20\text{--}100 \text{ GPa}$. The pertinent parameters for these experiments are listed in Table I. u_o denotes the measured flyer plate velocity, u_j denotes the measured jump-off velocity, and U_s denotes the measured shock velocity in the LD_2 . ρ'_0 and T'_0 indicate the estimated density and temperature states of the flyer plate at impact, as described in the previous section. The particle velocity u_p , the pressure P , and the density compression ρ_1/ρ_0 are inferred quantities, obtained as outlined in the text. The final four columns list weighted average values⁵¹ for U_s , u_p , P , and ρ_1/ρ_0 ; the experiments were divided into groups with common U_s , within $\sim 2\text{--}3\%$. It should be noted that the values of pressure listed in Table I are relative to an initial density of 0.17 g/cm^3 in order to make consistent comparisons with other published data.^{1,2,10–12,31–34} The actual pressures achieved are nominally of order $\rho_0/0.17 \approx 0.982$ lower due to the slightly lower initial density of $\sim 0.167 \text{ g/cm}^3$ in the present study.⁶²

The U_s - u_p and P - ρ_1/ρ_0 data obtained in the present study are plotted in Figs. 6 and 7. Also shown in Figs. 6 and 7 are data from Dick *et al.*³¹ (explosively driven), van Thiel *et al.*,^{32,33} and Nellis *et al.*³⁴ (gas gun), Da Silva *et al.*¹ and Collins *et al.*² (laser driven), Belov *et al.*,¹⁰ Boriskov *et al.*,¹¹

TABLE I. Principal Hugoniot data for LD_2 . u_v is the measured flyer plate velocity at impact, u_j is the measured jump-off velocity, ρ'_0 and T'_0 are the estimated density and temperature states of the flyer plate at impact, U_s is the measured shock velocity in the LD_2 sample, u_p is the inferred particle velocity in the LD_2 sample as determined by impedance matching, P is the inferred pressure, and ρ_1/ρ_0 is the inferred density compression of the LD_2 sample in the shocked state. The final four columns display weighted averages of the individual data points for U_s , u_p , P , and ρ_1/ρ_0 .

Expt. No.	Flyer plate	u_v (km/s)	u_j (km/s)	ρ'_0 (g/cm ³)	T'_0 (K)	U_s (km/s)	u_p (km/s)	P (GPa)	ρ_1/ρ_0	Weighted averages			
										U_s (km/s)	u_p (km/s)	P (GPa)	ρ_1/ρ_0
Z904N	Ti	9.48±0.07	0	4.417	300	13.5±0.24	9.68±0.24	22.2±0.6	3.53±0.28	13.55±0.18	9.68±0.17	22.3±0.5	3.50±0.20
Z904S	Ti	9.49±0.07	0	4.417	300	13.61±0.27	9.69±0.24	22.4±0.7	3.47±0.28				
Z590	Ti	11.48±0.34	0	4.417	300	15.26±0.28	11.73±0.52	30.4±1.4	4.32±0.70	15.69±0.11	11.77±0.14	31.4±0.4	3.98±0.18
Z895N	Ti	11.58±0.12	0	4.417	300	15.41±0.39	11.84±0.32	31.0±1.1	4.31±0.56				
Z895S	Ti	11.48±0.11	0	4.417	300	15.72±0.39	11.69±0.31	31.3±1.1	3.90±0.43				
Z698	Al	12.87±0.13	0	2.699	300	15.78±0.15	11.69±0.21	31.4±0.6	3.86±0.23				
Z592	Ti	12.23±0.37	0	4.417	300	15.99±0.31	12.47±0.55	33.9±1.6	4.55±0.80				
Z792S	Al	15.10±0.15	4	2.638	587	17.91±0.39	13.50±0.24	41.1±1.1	4.06±0.37	18.18±0.05	13.72±0.13	42.3±0.5	4.21±0.16
Z824S	Ti	13.73±0.10	2.2	4.407	408	17.97±0.11	13.93±0.33	42.6±1.0	4.45±0.38				
Z792N	Al	15.15±0.15	2.3	2.685	381	17.98±0.40	13.64±0.24	41.7±1.1	4.14±0.40				
Z824N	Ti	13.55±0.10	2.2	4.407	408	18.02±0.10	13.74±0.33	42.1±1.0	4.21±0.34				
Z1108	Ti	13.80±0.14	3	4.389	530	18.34±0.10	13.93±0.37	43.4±1.2	4.16±0.36				
Z593	Ti	14.06±0.42	0	4.417	300	18.63±0.15	14.26±0.62	45.2±2.0	4.27±0.62				
Z634	Al	19.77±0.20	6.1	2.498	913	22.48±0.19	17.08±0.30	65.3±1.2	4.16±0.26	22.48±0.19	17.08±0.30	65.3±1.2	4.16±0.26
Z711	Al	20.43±0.31	5	2.585	738	23.23±0.19	17.85±0.39	70.5±1.6	4.32±0.34	23.33±0.10	17.70±0.14	70.3±0.6	4.12±0.12
Z710	Al	20.18±0.20	5	2.585	738	23.25±0.19	17.64±0.31	69.7±1.3	4.14±0.26				
Z1109S	Ti	17.91±0.13	4.5	4.327	879	23.30±0.36	17.72±0.42	70.2±1.9	4.18±0.39				
Z1109N	Ti	17.91±0.13	4.5	4.327	879	23.43±0.38	17.80±0.42	70.9±2.0	4.16±0.39				
Z712	Al	20.30±0.15	5.4	2.557	801	23.45±0.22	17.65±0.27	70.4±1.2	4.05±0.23				
Z791S	Al	20.30±0.41	5.4	2.425	1022	23.49±0.41	17.65±0.46	70.5±2.1	4.02±0.40				
Z791N	Al	20.30±0.41	5.4	2.425	1022	23.57±0.50	17.64±0.46	70.7±2.3	3.98±0.42				
Z894	Ti	18.56±0.09	4.7	4.316	937	24.10±0.22	18.43±0.40	75.5±1.7	4.25±0.33	24.28±0.17	18.42±0.28	76.2±1.3	4.11±0.22
Z893	Ti	18.60±0.09	4.5	4.327	879	24.56±0.27	18.42±0.40	76.9±1.8	4.00±0.30				
Z1111N	Ti	19.23±0.10	0	4.417	300	24.94±0.44	19.17±0.42	81.3±2.2	4.33±0.43	25.11±0.32	19.15±0.30	81.8±1.3	4.21±0.28
Z1111S	Ti	19.23±0.10	0	4.417	300	25.30±0.46	19.14±0.42	82.3±2.2	4.11±0.38				
Z1110N	Ti	20.22±0.10	0	4.417	300	26.11±0.47	20.12±0.44	89.3±2.4	4.36±0.44	26.26±0.34	20.11±0.31	89.8±1.7	4.26±0.29
Z1110S	Ti	20.22±0.10	0	4.417	300	26.44±0.50	20.09±0.44	90.3±2.4	4.16±0.40				
Z946	Ti	22.38±0.69	8.7	3.8	2200	28.00±0.57	21.22±0.93	101.0±4.8	4.13±0.64	28.00±0.57	21.22±0.93	101.0±4.8	4.13±0.64

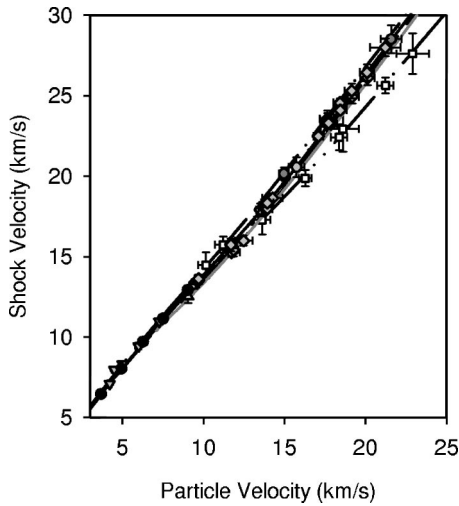


FIG. 6. LD_2 U_s - u_p Hugoniots. Theoretical models: Kerley 03 [solid black line (Ref. 37)]; Sesame 72 [dot-dashed line (Ref. 3)]; TB [dotted line (Ref. 19)]; GGA-MD [solid gray line (Ref. 20)]; Desjarlais [dashed line (Ref. 23)]; PIMC [open circles (Ref. 16)]; Ross [dot-dot-dashed line (Ref. 28)]. Experiments: Nellis *et al.* [black circles (Ref. 34)]; van Thiel *et al.* [gray triangles (Refs. 32, 33)]; Dick *et al.* [inverted gray triangles (Ref. 31)]; Laser-driven [open squares (Refs. 1,2)]; Convergent geometry [gray circle initially liquid sample (Ref. 12), dark gray circles initially solid samples (Refs. 10,11)]; this work (gray diamonds).

and Trunin *et al.*¹² (convergent geometry). Several theoretical model predictions are also plotted: Sesame 72,³ Ross,²⁸ and Kerley 03 (Ref. 37) (chemical picture); TB,¹⁹ PIMC,¹⁶ GGA-MD,²⁰ and Desjarlais²³ (*ab initio*).

Several points are apparent from these comparisons. First, as alluded to above, only relatively slight differences are observed between the directly measured U_s - u_p observables in all of these experiments. These differences are magnified when the results are projected into the P - ρ_1/ρ_0 plane. Second, the lowest pressure experiments in the present study were found to be in good agreement with results reported from earlier explosively driven and gas gun experiments, as

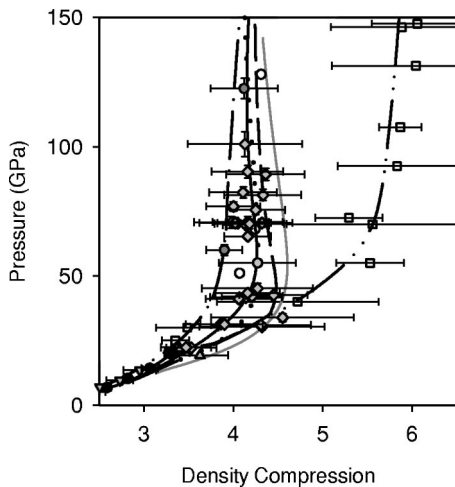


FIG. 7. LD_2 pressure-density compression Hugoniots. Lines and symbols as in Fig. 6.

well as the lowest pressure laser experiments. However, at higher pressures, particularly in the 70–100 GPa range, there is a distinct deviation between the present results and those reported from the laser-driven experiments. Contrary to the laser-driven experiments and the Ross model, the present results indicate that the Hugoniot stiffens at pressures near ~ 40 – 50 GPa, in good agreement with all of the *ab initio* models, and the Sesame 72 and Kerley 03 models.

The results from Belov *et al.*, Boriskov *et al.*, and Trunin *et al.*, shown as weighted average points in Figs. 6 and 7, agree with the stiffer response observed in the present experiments. Given the fact that these experiments used completely independent experimental configurations, the agreement of the inferred density compression makes a strong case for a ~ 4.3 - to ~ 4.5 -fold limiting compression for the equilibrium response of LD_2 along the principal Hugoniot. However, a caveat is that both experiments utilize the impedance matching method, and thus rely on accurate release isentropes for aluminum. Nevertheless, this agreement is encouraging given the release studies performed on aluminum by Russian investigators.⁶³ For completeness, it should be noted that the results at ~ 60 and ~ 120 GPa were obtained for deuterium initially in the solid state, with a density of ~ 0.199 g/cm³. Due to this elevated initial density one would expect $\sim 5\%$ lower density compression compared to an initially liquid state with density ~ 0.17 g/cm³.⁶⁴

B. Reverberating wave experiments

A total of 19 reverberating wave experiments were performed on LD_2 over a pressure range of ~ 20 – 80 GPa. The pertinent parameters for these experiments are listed in Table II. U_s denotes the measured shock velocity in the LD_2 and t_i/t_r denotes the measured reverberation ratio (initial transit time divided by the reverberation time). The final two columns list weighted average values for U_s and t_i/t_r , again with experiments divided into groups with common U_s , within ~ 2 – 3% .

Results of reverberating wave measurements at several initial pressure states are plotted in Fig. 8. We chose to plot the initial shock velocity in the LD_2 U_{s1} (increase in U_{s1} correlates to an increase in P) as a function of the reverberation ratio t_i/t_r (increase in t_i/t_r correlates to an increase in ρ_1 and thus ρ_1/ρ_0) to allow for a clearer comparison with the P - ρ_1/ρ_0 principal Hugoniot shown in Fig. 7. Also shown in Fig. 8 are several predictions for various LD_2 models: Sesame 72,³ Young,³⁰ and Kerley 03 (Ref. 37) (chemical picture); TB,¹⁹ GGA-MD,²⁰ and Desjarlais²³ (*ab initio*). We note that the PIMC (Ref. 16) predictions are not plotted; the PIMC results, in its region of applicability (above ~ 50 GPa), are very similar to the Kerley 03 predictions. We also note that the Ross²⁸ model predictions (not shown) are very similar to the Young model predictions over the entire region of interest. All model predictions were obtained using the Sesame 3700 (Ref. 54) and 7411 (Ref. 65) EOS models for aluminum and sapphire, respectively. The uncertainties in the model predictions due to the particular EOS models used will be discussed in Sec. V.

TABLE II. Reverberating wave data for LD_2 . U_s is the measured shock velocity in the LD_2 sample and t_i/t_r is the measured reverberation ratio. The final two columns display weighted averages of the individual data points.

Expt. No.	U_s (km/s)	t_i/t_r	Weighted averages	
			U_s (km/s)	t_i/t_r
Z904N	13.50 ± 0.24	2.79 ± 0.19	13.50 ± 0.24	2.79 ± 0.19
Z895S	15.72 ± 0.39	3.15 ± 0.30	15.81 ± 0.13	3.29 ± 0.13
Z698	15.78 ± 0.15	3.35 ± 0.17		
Z592	15.99 ± 0.31	3.24 ± 0.32		
Z792S	17.91 ± 0.39	3.48 ± 0.18	18.18 ± 0.08	3.39 ± 0.07
Z792N	17.98 ± 0.40	3.48 ± 0.18		
Z762N	18.00 ± 0.36	3.37 ± 0.17		
Z824N	18.02 ± 0.10	3.44 ± 0.18		
Z762S	18.15 ± 0.54	3.32 ± 0.17		
Z593	18.63 ± 0.15	3.32 ± 0.14		
Z634	22.48 ± 0.19	3.03 ± 0.27	22.48 ± 0.19	3.03 ± 0.27
Z711	23.23 ± 0.19	3.01 ± 0.26	23.33 ± 0.10	3.08 ± 0.09
Z710	23.25 ± 0.19	2.94 ± 0.26		
Z1109N	23.43 ± 0.38	3.14 ± 0.25		
Z712	23.45 ± 0.22	3.00 ± 0.27		
Z791S	23.49 ± 0.41	3.13 ± 0.18		
Z791N	23.57 ± 0.50	3.15 ± 0.18		
Z894	24.10 ± 0.22	3.06 ± 0.23	24.10 ± 0.22	3.06 ± 0.23
Z1111N	24.94 ± 0.44	3.20 ± 0.26	24.94 ± 0.44	3.20 ± 0.26

Several points are apparent from these comparisons. First, the measured reverberation ratio at the lowest pressure (~ 20 GPa) is in good agreement with the predictions of nearly all of the models (TB and GGA-MD being possible exceptions). This is expected since all of the models, except for the TB and GGA-MD models where little attention was paid to low pressures, agree well with the gas gun Hugoniot results.^{32–34} Second, the measured ratios indicate an increase in shock compression over the predictions of the Sesame 72 model between ~ 30 – 60 GPa. Third, the measured ratios above ~ 40 – 50 GPa suggest a definite stiffening of the principal Hugoniot above ~ 40 – 50 GPa, in accordance with the principal Hugoniot measurements. In particular, the data at the highest shock velocities, corresponding to ~ 70 – 80 GPa, are in excellent agreement with all of the *ab initio* models, as well as the Sesame 72 and Kerley 03 models. This agreement corroborates the principal Hugoniot results obtained through the impedance matching experiments. If the density compression was \sim sixfold along the Hugoniot, as indicated by the laser-driven experiments,^{1,2} t_i/t_r would continue to increase with increasing pressure, commensurate with the predictions of the Young model. The fact that t_i/t_r is observed to decrease slightly from ~ 45 to ~ 75 GPa is strong supporting evidence that ~ 4.5 -fold compression is not exceeded along the principal Hugoniot, and that the Hugoniot begins

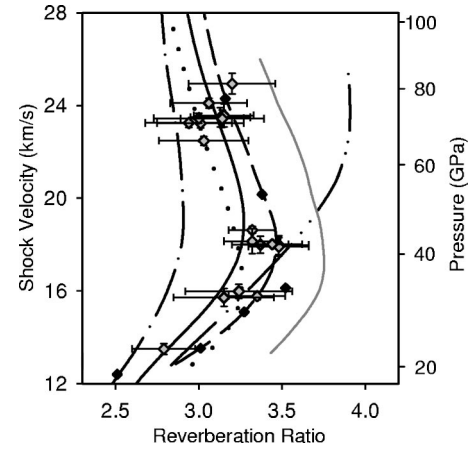


FIG. 8. Measured reverberation ratio compared with theoretical predictions. Lines and symbols as in Fig. 6, with one exception; in this figure the dot-dot-dashed line is the Young model (Ref. 30), which is very similar in behavior to the Ross model (Ref. 28). Black diamonds indicate individual calculations of Desjarlais (Ref. 23).

to stiffen at pressures above ~ 45 GPa. Furthermore, the maximum in t_i/t_r observed at ~ 45 GPa implies that a maximum in the density compression along the Hugoniot occurs at ~ 45 GPa, which is also consistent with the principal Hugoniot determined from impedance matching. Using the arguments outlined in the previous section [discussion of Eq. (1)], this maximum in compression is approximately 4.5- to 4.7-fold, in good agreement with the ~ 4.3 -fold maximum inferred from impedance matching.

These reverberating wave measurements also provide data to discriminate, to a first approximation, between some of the stiffer EOS models in the pressure range of 25–50 GPa. The impedance matching Hugoniot measurements over this pressure range are unable to distinguish between the various stiffer EOS models, all of which fall within the scatter and uncertainty of the measurements. However, the differences in model predictions for the reverberation ratio in this pressure range are significantly larger and exceed the measurement scatter and uncertainty. In particular, our data exhibit the best agreement with the Kerley 03 and Desjarlais models. The Sesame 72 model is clearly too stiff between ~ 30 – 60 GPa. The GGA-MD model is too soft throughout most of the region of interest. The TB model, while exhibiting good agreement throughout most of the pressure range of interest, is slightly too soft at pressures just above the gas gun limit (~ 20 GPa).

C. Reshock experiments

A total of 15 mechanical reshock experiments were performed on LD_2 over an initial shock pressure range of ~ 20 – 100 GPa (final reshock pressures of ~ 70 – 400 GPa). The pertinent parameters for these experiments are listed in Table III. Columns two through five list the measured shock velocity U_s of the LD_2 sample, the aluminum (6061-T6) anvil, the z -cut sapphire anvil, and the z -cut α -quartz anvil, respectively. The final two columns list the inferred pressure P_2 and density ρ_2 for the reshocked deuterium.

TABLE III. Reshock data for LD_2 using several different anvils. Columns two through five display the measured shock velocity in the singly shocked LD_2 , aluminum, sapphire, and z -cut α -quartz samples, respectively. The final two columns display the inferred pressure P_2 and density ρ_2 for the reshocked deuterium.

Expt. No.	LD_2 U_s (km/s)	Al U_s (km/s)	Sapphire U_s (km/s)	α -quartz U_s (km/s)	P_2 (GPa)	ρ_2 (g/cc)
Z904N	13.50±0.24		10.58±0.15		82.1±6.3	1.42±0.37
Z904S	13.61±0.27	9.29±0.21			66.2±5.9	1.69±0.65
Z824S	17.97±0.11		13.12±0.20		210.0±11.7	1.31±0.22
Z824N	18.02±0.10	12.22±0.24			167.0±9.8	1.23±0.20
Z1108	18.34±0.10			11.50±0.36	183.2±13.2	1.01±0.14
Z1109S	23.30±0.36			13.62±0.41	269.3±18.2	1.10±0.18
Z1109N	23.43±0.38		14.50±0.44		297.1±29.7	1.36±0.32
Z894	24.10±0.22		14.86±0.22		321.8±15.4	1.37±0.24
Z893	24.56±0.27	14.58±0.36			276.0±18.5	1.19±0.20
Z1111N	24.94±0.44		15.55±0.46		371.6±34.2	1.27±0.26
Z1111S	25.30±0.46			14.60±0.44	314.5±21.1	1.07±0.17
Z1110N	26.11±0.47		15.70±0.47		382.8±35.4	1.41±0.33
Z1110S	26.44±0.50	15.23±0.46			310.5±25.0	1.39±0.34
Z946N	28.00±0.57		15.95±0.45		401.9±34.6	1.39±0.50
Z946S	28.00±0.57	16.45±0.49			380.1±29.3	1.15±0.33

The reshock data for sapphire anvils are plotted in Fig. 9, as shock velocity in the sapphire versus initial shock velocity in the LD_2 . Also shown in Fig. 9 are predictions from various LD_2 models: Sesame 72,³ Ross,²⁸ and Kerley 03 (Ref. 37) (chemical picture); TB¹⁹ and Desjarlais²³ (*ab initio*). Again, the PIMC (Ref. 16) predictions are not plotted since they are very similar to the Kerley 03 predictions for shock velocities above 20 km/s. All model predictions were obtained using the Sesame 7411 (Ref. 65) EOS model for sapphire. The uncertainties in the model predictions due to the particular EOS model used for sapphire will be discussed in Sec. V.

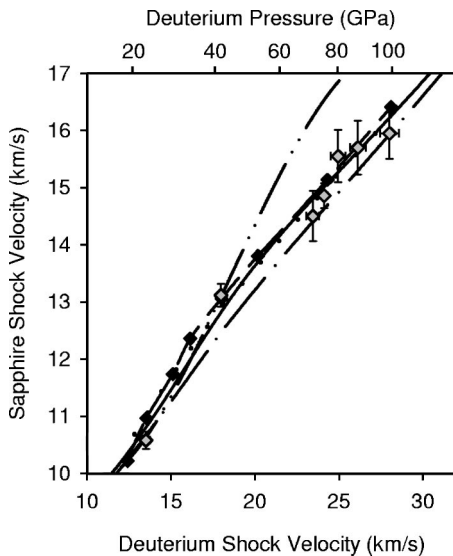


FIG. 9. Measured shock velocity in sapphire upon LD_2 reshock as a function of initial shock velocity in LD_2 . Lines and symbols as in Fig. 6. Black diamonds indicate individual calculations of Desjarlais (Ref. 67).

The lowest pressure experiment, which corresponds to ~ 22 GPa, is in good agreement with all of the models. As in the reverberating wave experiments, this is expected since all of the models are in relatively good agreement with the gas gun Hugoniot data.^{32–34} As the pressure increases, particularly above ~ 40 – 45 GPa ($U_s \approx 18$ – 20 km/s), the predicted shock velocities in the sapphire, and thus the reshock pressures in the LD_2 , diverge. If we consider the Sesame 72 and Ross models as the extremes (Sesame 72 exhibits the stiffest response while Ross exhibits the softest response), the other models shown tend to follow the Ross model to initial LD_2 shock velocities of ~ 18 km/s. However above ~ 18 km/s these models shift over to a response that is more indicative of the Sesame 72 model. The experimental data also appear to follow this trend. Similar to the principal Hugoniot and reverberating wave results, this trend is indicative of an enhanced shock compression relative to the Sesame 72 model in the ~ 20 – 40 GPa pressure range, followed by stiffening of the principal Hugoniot above ~ 40 – 50 GPa.

Similar trends are observed in the reshock response from aluminum and z -cut α -quartz anvils. These results are plotted in Figs. 10 and 11, along with the Sesame 72, Kerley 03, and Ross models. Predictions from the TB and Desjarlais models are not plotted. However, we note that GGA-MD and PIMC calculations performed for an aluminum anvil⁶⁶ and a single point from the Desjarlais model for a α -quartz anvil⁶⁷ exhibit the same general behavior as that seen for the sapphire anvil. All model predictions were obtained using the Sesame 3700 (Ref. 54) and 7360 (Ref. 68) EOS models for aluminum and α quartz, respectively. The uncertainties in the model predictions due to the particular EOS models used for aluminum and α quartz will be discussed in Sec. V.

We note that the results obtained in the aluminum experiments differ from that reported by Mostovych *et al.*^{6,7} (not shown), although the rather significant error bars and scatter

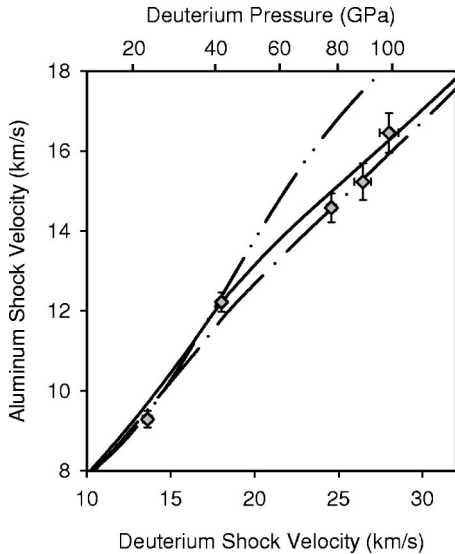


FIG. 10. Measured shock velocity in aluminum upon LD_2 reshock as a function of initial shock velocity in LD_2 . Lines and symbols as in Fig. 6.

of the data make the comparison difficult. Finally, we mention that the present results for the experiments with z -cut α -quartz anvils are in good agreement with similar measurements recently made at the Omega laser facility,¹³ over the pressure range of overlap (below ~ 80 GPa).

For completeness, we emphasize that the reshock measurement is inherently an integrated experiment, since the interpretation depends not only on the behavior of LD_2 along the principal Hugoniot, but also on the behavior of LD_2 upon reshock. Thus, conclusions regarding the principal Hugoniot are model dependent and cannot be unambiguously determined. For example, an observed reshock pressure could be obtained from a stiff response along the principal Hugoniot

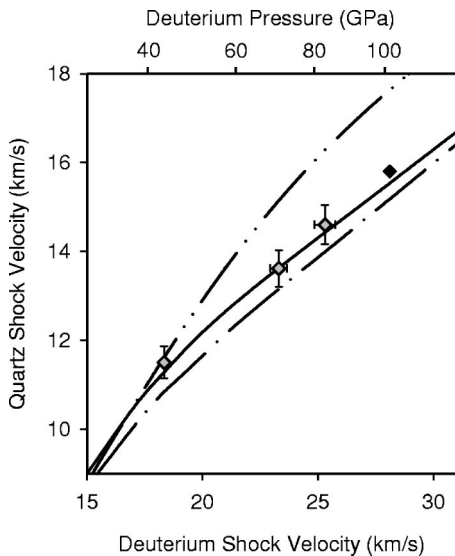


FIG. 11. Measured shock velocity in z -cut α quartz upon LD_2 reshock as a function of initial shock velocity in LD_2 . Lines and symbols as in Fig. 6. Black diamond indicates individual calculation of Desjarlais (Ref. 67).

followed by a stiff reshock response; alternatively it could also be obtained from a soft response along the principal Hugoniot followed by a soft reshock response. Nevertheless, the general behavior observed for all three sets of experiments (principal Hugoniot, reverberating wave, and reshock) further strengthens the conclusion of ~ 4.3 - to ~ 4.5 -fold limiting compression for the equilibrium response of LD_2 along the principal Hugoniot.

Note that since P_1 and ρ_1 are inferred from the impedance matching experiments, the measured shock velocity in the anvil material can also be used to infer the reshock pressure P_2 and the reshock density ρ_2 . These values are listed in the final two columns of Table III. The uncertainty in ρ_2 is rather large, due to the propagation of the uncertainty in ρ_1 and the anvil shock velocity U_{sA} . However, even with the significant uncertainty in ρ_2 , the inferred reshock densities further support the stiff Principal Hugoniot response.

IV. DISCUSSION

From the three sets of measurements made in this study (Hugoniot, reverberating wave, and reshock), a consistent picture emerges for the high-pressure response of deuterium. First, all three measurements are consistent with the gas gun Hugoniot results.³²⁻³⁴ This is significant in that due to the large sample sizes and long duration of constant pressure achievable in gas gun experiments, those results are considered highly accurate. Second, the present results between ~ 20 – 40 GPa are consistent with a somewhat higher density compression than that predicted by the earlier chemical picture models, such as the Sesame 72 model.³ This is evident in the reverberating wave and reshock experiments by the larger observed reverberation ratio and the higher observed anvil shock velocity, respectively. Third, there appears to be a maximum in compression along the principal Hugoniot at a pressure of ~ 40 – 50 GPa, consistent with ~ 4.3 - to ~ 4.5 -fold compression. This is evident in the reverberating wave experiments as a maximum in the observed reverberation ratio at ~ 40 – 50 GPa. Finally, above ~ 50 GPa there appears to be a definite stiffening of the principal Hugoniot, with the compression approaching fourfold. This is apparent in the reverberating wave experiments as a decrease in the observed reverberation ratio with increasing pressure, and in the reshock experiments as a transition from a behavior indicative of the Ross model²⁸ to that indicative of the Sesame 72 model. Given these correlations, these three sets of measurements are self-consistent.

We can also show explicitly the self-consistency of these measurements through a model-independent analysis. Consider the reshock pressure and the LD_2 initial shock velocity, two experimental observables, as fixed quantities. These parameters provide stringent constraints on the possible range of measurable reverberation ratios, based upon simple wave propagation arguments. For the following discussion refer to the P - u_p diagram shown in Fig. 12, which corresponds to the observables from shot Z824. The measured shock velocity U_{s1} requires the initial Hugoniot point to lie on a chord with slope given by $\rho_0 U_{s1}$. The density in the first shock state ρ_1 (which in this exercise is treated as an independent

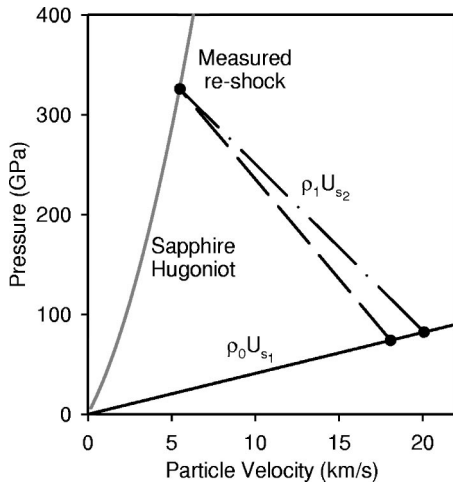


FIG. 12. Determination of densities and shock velocities from the pressure-particle velocity diagram. Shown are chords obtained for a first shock density compression of 4 (dashed line) and 6 (dot-dashed line). In this case the initial LD_2 shock velocity is 24.1 km/s and the reshock pressure is 321 GPa.

variable), will determine the particle velocity such that $(\rho_1/\rho_0) = U_{s1}/(U_{s1} - u_{p1})$, i.e., $u_{p1} = U_{s1}(1 - \rho_0/\rho_1)$. The measured reshock pressure then determines the chord connecting the first shock and second shock state. From this chord one can determine U_{s2} (i.e., the slope of the chord is $\rho_1 U_{s2}$) and ρ_2 [i.e., $(\rho_2/\rho_1) = U_{s2}/(U_{s2} - u_{p2})$]. Thus, the only unknown quantity necessary to determine the reverberation ratio is U_{s3} [see Eq. (1)]. If one makes the assumption that $U_{s3} = U_{s2}$ (a good assumption, based on the arguments presented in Secs. II and V), then t_i/t_r can be calculated as a function of ρ_1 , independent of any particular model for LD_2 .

Figure 13 shows such an analysis for a measured initial LD_2 shock velocity of 23.3 ± 0.1 km/s and a measured reshock pressure of 297 ± 27 GPa (corresponds to weighted average values for experiments at ~ 70 GPa). The solid black line and dashed black lines indicate the possible reverberation ratios for the measured reshock state of 297 GPa and the bounds at 270 and 324 GPa, respectively. Also shown on the plot are the measured density compression bounds obtained from the impedance matching Hugoniot measurements (vertical gray band between 4.0 and 4.24), and the measured reverberation ratio bounds (horizontal gray band between 2.99 and 3.17). We see that the possible reverberation ratios from the model-independent analysis is in good agreement with the experimental results, thus establishing the internal self-consistency of these three measurements. In contrast, the possible reverberation ratios for a reshock pressure of ~ 400 GPa (Ross model prediction for an initial LD_2 shock velocity of 23.3 km/s), shown as the solid gray curve in Fig. 13, is clearly outside of the acceptable experimental bounds. Similar consistency was observed for all of the initial pressure states at which we have all three sets of measurements.

The overall behavior observed in the present study is captured quite well by the recent models of Kerley³⁷ and Desjarlais.²³ The agreement of these two models with the

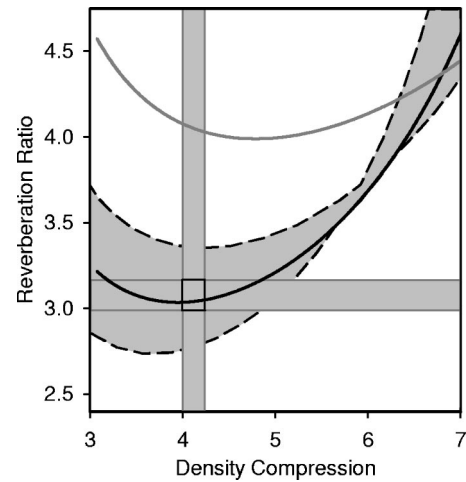


FIG. 13. Predicted reverberation ratio as a function of density compression for an initial LD_2 shock velocity of 23.3 km/s and a reshock pressure of 297 GPa ($\pm 9\%$) (solid black line bounded by dashed black lines). The measured reverberation ratio and density compression are indicated by the horizontal and vertical gray bands, respectively. The experimental data are bounded by the sides of the gray solid box. The predicted reverberation ratio for a reshock pressure corresponding to the Ross model (Ref. 28) is also shown for comparison (gray line).

present data set is best seen in comparison with weighted average representation of the individual data points. Groups of data with shock velocities within $\sim 2-3\%$ of each other were averaged with the weights being the inverse squares of the uncertainties.⁵¹ The resulting weighted average data points are listed in Tables I and II and shown graphically in Figs. 14 and 15, along with the predictions of the Kerley 03 and Desjarlais models.

Both models show good agreement with gas gun data and enhanced compression between $\sim 20-40$ GPa, evidently due to the onset of dissociation. This enhanced compression is quite apparent in the Desjarlais model, with a sudden increase in density reminiscent of a phase transformation. In-

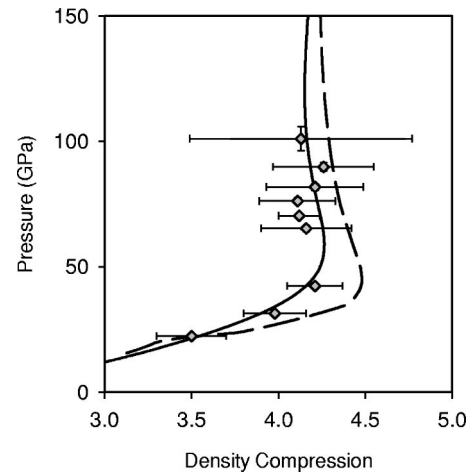


FIG. 14. LD_2 pressure-density compression Hugoniots, weighted average. Lines and symbols as in Fig. 6.

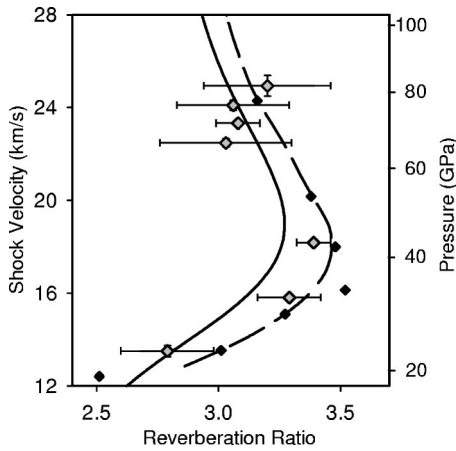


FIG. 15. Reverberation ratio, weighted average. Lines and symbols as in Fig. 6. Black diamonds indicate individual calculations of Desjarlais (Ref. 23).

deed, estimations of dissociation along the principal Hugoniot in the Desjarlais model show an abrupt drop in the bound fraction at pressures above ~ 20 GPa, commensurate with the abrupt increase in density.²³ The density increase is less abrupt for the Kerley 03 model. However, this model also predicts significant dissociation above ~ 20 GPa.³⁷ At higher pressures, both models are seen to stiffen abruptly at ~ 40 – 50 GPa, showing a maximum in shock compression followed by a decrease in compression as the pressure increases. We note that above ~ 100 GPa both models are in excellent agreement with the predictions of the PIMC model,¹⁶ a highly accurate *ab initio* treatment at these elevated temperatures and pressures. In fact, all of the models that show reasonable agreement with our results below ~ 100 GPa tend towards fourfold compression at higher pressures, which is the limiting compression expected for a monatomic ideal gas. The only models which exhibit enhanced compression above ~ 100 GPa are those that also predict enhanced compression at lower pressures. We note that this general behavior is in good agreement with recent arguments presented by Nellis.¹⁴

A few comments regarding the Kerley 03 and Desjarlais models are appropriate. As mentioned above, the Kerley 03 model is a complete revision of the Sesame 72 model. It retains the basic concepts and structure of the Sesame 72 model, but incorporates major improvements, particularly in the treatment of the liquid perturbation theory, the treatment of molecular vibrations and rotations, and the ionization equilibrium and mixture models. In addition, new experimental data and theoretical calculations were available to calibrate certain model parameters; in particular the zero-Kelvin isotherms for the molecular and atomic solids, and the quantum corrections to the liquid phase.³⁷ This model provides excellent agreement with the measured dynamical response obtained in the present study, and possibly more importantly, provides a good global EOS valid over a wide range of pressure, temperature, and density.

The Desjarlais model is a FT-DFT based *ab initio* model, in the same spirit of the previously published GGA-MD

model.²⁰ However, several improvements over the previous GGA-MD treatment were made; of most importance was the use of higher energy cutoffs to ensure convergence of not only the energy, but also the electronic pressure. Also important, but less so than the higher energy cutoffs, was the inclusion of the zero-point energy in the reference state. These improvements resulted in an overall stiffening of the Hugoniot response relative to the GGA-MD model. Notably, unlike the GGA-MD model, the Desjarlais model exhibits excellent agreement with the highest pressure gas gun data, a criticism of the prior *ab initio* treatments.⁶⁹ Being an *ab initio* based model, the Desjarlais model provides physical insight into the nature of the fluid and allows for estimation of optical and electrical properties in addition to the mechanical properties. However, since calculations have only been performed for comparison with principal Hugoniot and reverberating wave experiments,²³ the current model is only valid in a relatively narrow pressure, temperature, and density range.

V. COMMENTS REGARDING UNCERTAINTY AND POTENTIAL SYSTEMATIC ERRORS

The present experimental results disagree with previous results obtained in laser-driven experiments.^{1,2,6,7} In particular, the inferred density compression along the Hugoniot and the reshock pressure obtained in experiments using aluminum anvil materials suggest a stiffer Hugoniot than that determined from the laser-driven experiments. Since both sets of data (i.e., laser-driven and magnetically-driven flyer plate) cannot be correct, at least one of the two experimental data sets must be in error. This assertion is not inconceivable, considering that both of these experimental techniques are relatively new and have not been established over a wide range of experimental conditions. Therefore, we have taken special care to rule out the existence of systematic errors in our work. In this section we discuss each set of experiments separately and comment on the potential sources of systematic errors, the possible magnitude of these potential errors, and what has been done to mitigate and/or determine that such systematic errors are likely not present.

A. Principal Hugoniot experiments

The most significant source of potential systematic error in the impedance matching experiments is the accuracy of the aluminum EOS, the standard used in the present principal Hugoniot experiments, under both compression and release. Aluminum is one of the most widely studied metals under compression, thus a significant data base exists to define the Hugoniot of aluminum over the pressure range of interest in this study (~ 200 – 700 GPa). In particular, the magnetically driven flyer technique was used to obtain near-symmetric impact experiments on aluminum to stresses up to ~ 500 GPa,⁴¹ in part to validate this technique for performing high-pressure EOS experiments. More recently these measurements have been extended to initial shock stresses over 700 GPa in truly symmetric impact experiments. The results of these experiments suggest that the Sesame 3700 model⁵⁴ for aluminum provides a good description of the

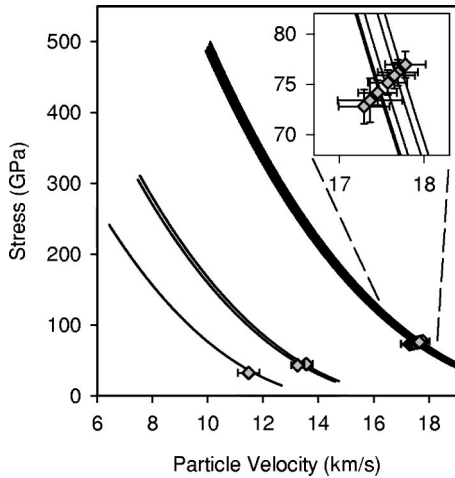


FIG. 16. Release measurements in aluminum. Solid lines are calculated release paths from Sesame 3700 (Ref. 54), symbols are experimental measurements using 200 mg/cm^3 silica aerogel. Inset included for more detail.

response of aluminum under compression (see Ref. 41). Thus the remaining question relates to the accuracy to which the aluminum release isentrope from high-stress states can be determined.

To determine the accuracy of the calculated release isentrope of aluminum, release experiments were performed for initial shock stresses ranging from ~ 250 – 500 GPa, using a low density (200 mg/cm^3) silica aerogel. This technique is similar to that used by Holmes to measure the aluminum release from ~ 80 GPa, to an accuracy of $\sim 1\%$ in u_p .⁷⁰ Direct impact experiments were performed to generate Hugoniot data for aerogel in the range of ~ 30 – 75 GPa. Experiments were then performed in which a shock was transmitted from the aluminum drive plate into the silica aerogel, which simulates unloading to the LD_2 state. The measured U_s for the aerogel in the release experiment, along with the measured aerogel Hugoniot, determines a point in P - u_p space through which the aluminum release isentrope must pass. A total of ten release experiments were performed, in which release points in aluminum were measured from initial shock states in the range of ~ 250 – 500 GPa. The results of these experiments are plotted in Fig. 16, along with aluminum release calculations from the Sesame 3700 model for aluminum.⁵⁴ The agreement between experiment and calculation is within experimental uncertainty over this entire range. Thus, these measurements validate the Sesame 3700 release behavior over the pressure range of interest in this study, and indicate that no significant errors in the inferred LD_2 density are a result of the aluminum EOS. In particular, statistical analysis of the ten experiments indicate no evidence of a systematic soft or stiff response in the release behavior of Sesame 3700, and that the predicted particle velocity for the release state is accurate to within $\sim 1\%$. This level of agreement translates to an accuracy in the inferred density compression of ~ 3 – 3.5% , which agrees very well with the scatter observed in the data groupings listed in Table I.

Other potential sources of error in the principal Hugoniot experiments could include steadiness and planarity of the pressure generated by the magnetically driven flyer plate impact. The constancy of both the VISAR and self-emission profiles from the shock front (see Fig. 2) over the duration of the experiment indicates that the pressure remains constant to better than ~ 1 – 2% over the full time duration of the Hugoniot experiment; the intensity of the self-emission is proportional to the pressure of the LD_2 to the ~ 1.75 power.⁷¹ Further, the planarity of impact in the magnetically driven flyer experiments has been studied, both through experiment and simulation (see Refs. 41,43). Results of these studies indicate that the flyer plate is planar to within $\sim 30 \mu\text{m}$ over roughly 3 mm width at impact (corresponding to an effective tilt of $\sim 10 \text{ mrad}$), and within ~ 5 – $10 \mu\text{m}$ at $\sim 2 \text{ mm}$ width (~ 2 – 5 mrad). This is typical of the impact tilt in conventional gas gun experiments, which often quote uncertainties of less than 1% .

B. Reverberating wave experiments

Unlike the Hugoniot experiments, the reverberating wave experiment is only weakly influenced by the accuracy of the aluminum EOS. In mapping the various LD_2 model predictions onto Fig. 8, an uncertainty in the aluminum EOS would result in very slight shifts of the predicted curves. The aluminum EOS influences the predicted reverberation ratio through the determination of the third shock velocity U_{s3} . Analysis of Eq. (1) indicates that the variation in the sensitivity of the reverberation ratio to uncertainties in U_3 goes as

$$\delta\left(\frac{t_i}{t_r}\right) / \left(\frac{t_i}{t_r}\right) \approx \frac{1}{3} \frac{\delta U_{s3}}{U_{s3}}. \quad (2)$$

Thus, the reverberation ratio is quite insensitive to the aluminum EOS. In particular, a 2 – 3% variation in U_{s3} , which is a reasonable estimate of the variation in U_{s3} that would result from using various aluminum EOS models,^{72–75} would result in only $\sim 1\%$ variation in the predicted reverberation ratio. Furthermore, if one considered a ~ 10 – 15% softer release response for aluminum, the magnitude required for the present impedance matching method to produce results in agreement with the density compression inferred in the laser-driven experiments, the resulting change in the predicted reverberation ratios would only be $\sim 3\%$. In contrast, the measured reverberation ratios at ~ 70 – 80 GPa are of order 25% lower than the predictions of the Young³⁰ or Ross²⁸ models.

The reverberating wave experiment is somewhat more sensitive to uncertainties in the sapphire EOS, which determines both the second shock velocity U_{s2} and the second shock density ρ_2 . Again, analysis of Eq. (1) indicates that the variation in the reverberation ratio goes as

$$\delta\left(\frac{t_i}{t_r}\right) / \left(\frac{t_i}{t_r}\right) \approx \frac{\delta u_{pA}}{u_{pA}}, \quad (3)$$

where $\delta u_{pA}/u_{pA}$ is the uncertainty in sapphire anvil particle velocity for a given sapphire shock velocity. While there is limited Hugoniot data for sapphire in the pressure range of 200 – 400 GPa, this uncertainty should only be of order

1–2%. In particular, the sapphire EOS used to obtain the predicted reverberation ratios is likely adequate, based upon the similarities in the observed reshock behavior of LD_2 inferred from sapphire, aluminum, and α -quartz anvil materials. This point will be discussed further below. Again, this uncertainty would manifest itself as slight shifts, of order 1–2%, in the predicted curves for the various models that appear in Fig. 8.

A final potential source of systematic error in the reverberating wave experiment is the steadiness of the shock over the full timescale of the experiment. The position-time plot shown in Fig. 4 demonstrates the need for constant pressure at the LD_2 /sapphire interface for times on order of ~ 30 – 40 ns in these experiments. The constancy of the self-emission signal shown in Fig. 4 during the initial transit time and the reverberation time suggests that the pressure does remain constant over the timescale necessary, at least for that experiment (experiment Z824). However, due to opacity effects in the sapphire window at higher reshock pressures, it was not always possible to evaluate the constancy of pressure during the reverberation time from self-emission measurements.

To determine the effect of constant pressure dwell time on the expected reverberation ratio, a series of hydrodynamic simulations were performed for an initial pressure state in the LD_2 of ~ 70 GPa, using both the Young³⁰ and the Kerley 03 (Ref. 37) models. In these simulations the initial flyer plate thickness was varied from 175 to 500 μm , which effectively varied the constant pressure dwell time in the simulations. The results of the simulations indicate that for effective flyer thicknesses greater than ~ 225 – 250 μm , the resulting reverberation ratio was unchanged. For thicknesses less than ~ 225 μm , the release wave emanating from the rear of the flyer plate causes the aluminum/ LD_2 interface to slow down prior to interaction with the oncoming reflected wave from the LD_2 /sapphire interface, resulting in a longer reverberation time. It was found that in order to reproduce the measured reverberation ratio using a soft EOS for LD_2 , such as the Young model, an effective flyer thickness of ~ 175 μm was required.

Magnetohydrodynamic (MHD) simulations indicate that at least ~ 300 μm of the original flyer thickness remains unaffected by magnetic diffusion upon impact of the flyer at the target.⁴³ Thus, these simulations suggest there are no effects of attenuation in the present reverberating wave experiments. However, more pragmatic bounds can be placed on the flyer thickness from experiments performed on LD_2 , silica aerogel, and aluminum. In the LD_2 hydrodynamic simulations, a flyer of at least ~ 200 μm thickness was required to ensure that the release from the rear of the flyer did not overtake the initial shock wave in the LD_2 prior to the shock reaching the LD_2 /sapphire interface. Given that no drop in the self-emission signal was observed during the initial transit time in any of the present experiments, the flyer thickness must have been at least ~ 200 μm . Similarly, the experiments performed on silica aerogel require flyer plate thicknesses of at least ~ 225 μm . Finally, previously reported symmetric impact experiments performed on aluminum⁴¹ require at least ~ 250 μm of flyer thickness.

These experimental results provide a more convincing argument that the present reverberating wave experiments are either unaffected, or only slightly influenced, by attenuation effects.

C. Reshock experiments

The most significant source of potential systematic error in the reshock experiments is the uncertainty in the EOS of the anvil material under compression. In mapping the various model predictions onto Figs. 9–11, any uncertainty in the anvil EOS would result in slight shifts of the predicted anvil shock velocity curves for the various models. However, the predicted shock velocity of the anvil is only weakly sensitive to uncertainties in the anvil EOS. It can be shown that variations in the predicted anvil shock velocity U_{S_A} go as

$$\frac{\delta U_{S_A}}{U_{S_A}} \approx \frac{1}{2} \frac{\delta u_{pA}}{u_{pA}}, \quad (4)$$

where $\delta u_{pA}/u_{pA}$ is the uncertainty in the anvil particle velocity for a given anvil shock velocity.

As mentioned above, the aluminum EOS under compression is very well known. Likewise, the EOS of z -cut α quartz under compression is well known; quartz has commonly been used as a standard in several high-pressure experiments.⁷⁶ Sapphire is the least well known of these anvil materials, at least in the pressure range of interest in this study (~ 85 – 400 GPa). However, considering the relatively low impedance of LD_2 compared to aluminum, quartz, and sapphire, the similarity in the reshock behavior of LD_2 inferred from the present experiments using these three anvil materials indicates that Sesame 7411 model for sapphire,⁶⁵ used in the present comparisons, is likely an accurate EOS in this high pressure regime. Furthermore, recent sapphire Hugoniot experiments between ~ 1000 – 2000 GPa (Ref. 77) show reasonable agreement with Sesame 7411, albeit these measurements are at significantly higher pressures than those achieved in the present work (~ 400 GPa).

VI. CONCLUSIONS

Using a magnetically driven flyer plate technique, the high-pressure response of LD_2 has been studied to pressures of ~ 400 GPa and densities of ~ 1.5 g/cm^3 . Using an impedance matching method, Hugoniot measurements were obtained in the pressure range of ~ 20 – 100 GPa. Results of these experiments suggest a stiff response of LD_2 shocked to pressures up to 100 GPa, with a peak density compression along the Hugoniot of approximately 4.3. The stiff Hugoniot response observed in the impedance matching experiments was confirmed in simultaneous, independent measurements of the relative transit times of shock waves reverberating with the sample cell. Results from the reverberating wave experiments suggest a peak compression along the principal Hugoniot of ~ 4.5 , in good agreement with the impedance matching result of ~ 4.3 . Finally, reshock measurements of LD_2 using sapphire, aluminum, and α -quartz anvils further corroborate this stiff response.

These measurements, principal Hugoniot, reverberating wave, and mechanical reshock, were shown to be internally self-consistent through a model-independent analysis. The individual results, taken as a whole, provide a consistent picture for the high-pressure response of LD_2 . Slightly above the upper end of the gas gun results,^{32–34} between ~ 20 – 40 GPa, an increase in shock compression is observed, which is somewhat larger than that predicted by the earlier chemical picture models,^{3–5} such as the Sesame 72.³ There appears to be a maximum in compression along the principal Hugoniot at a pressure of ~ 40 – 50 GPa. This maximum is consistent with ~ 4.3 - to ~ 4.5 -fold compression. Finally, above ~ 50 GPa there appears to be a definite stiffening of the principal Hugoniot. These trends in the experimental results are in excellent agreement with the Kerley 03 model,³⁷ a recent complete revision of the Sesame 72 chemical picture model, and the recent FT-DFT based *ab initio* model by Desjarlais.²³ This general behavior also supports recent arguments presented by Nellis concerning the high-pressure response of hydrogen and deuterium.¹⁴

We note that the results of the present work are also found to be in good agreement with recent experimental results up to ~ 100 GPa obtained using convergent geometry techniques.^{10–12} However, our results are in disagreement with previously reported results from laser-driven experiments.^{1,2,6,7} This disagreement prompted a careful consideration of potential systematic errors associated with each of the three experiments performed in this study. In particular, we assessed the constancy of the pressure drive through the VISAR and self-emission measurements, the effects of uncertainty in the EOS of the anvil materials, and the accuracy of the impedance matching technique through silica aerogel experiments. The results of all of these studies indicate that the conclusions drawn from the measurements described here are internally self-consistent, and are likely not significantly influenced by systematic errors.

ACKNOWLEDGMENTS

The authors would like to thank the large team at Sandia that contributed to the design and fabrication of the flyer plate loads and shock experiments, and the fielding of the cryogenics and the shock diagnostics. G.I. Kerley and M.P. Desjarlais are also thanked for numerous discussions concerning the high-pressure response of LD_2 . Sandia is a multiprogram laboratory operated by Sandia Corporation a Lockheed Martin Company, for the U.S. DOE under Contract No. DE-AC04-94AL8500.

APPENDIX: HUGONIOT UNCERTAINTY ANALYSIS

The uncertainties in the LD_2 particle velocity u_p , pressure P , and density compression ρ_1/ρ_0 , listed in Table I correspond to the uncertainties resulting from random errors in the determination of the LD_2 shock velocity U_s and the aluminum drive plate particle velocity u_{pAl} . The uncertainties listed in Table I do not include contributions due to the

accuracy of the calculated aluminum release response; it was shown that the Sesame 3700 (Ref. 54) model adequately represented the release response of aluminum (see Sec. V). Since the result of a systematic error in the release response would be slight shifts, of order a few percent, in the inferred density compression, and since these shifts would be nominally the same amount for each data point, it was deemed appropriate to treat the potential error in the density inference due to the accuracy of the calculated release response separately, as discussed in Sec. V. The discussion presented here relates to the uncertainties in u_p , P , and ρ_1/ρ_0 resulting from uncertainties in U_s and u_{pAl} .

U_s was a measured quantity in the experiment, and thus the uncertainty in U_s was determined by the accuracy in which the shock velocity could be inferred from the experimental records, which was typically ~ 0.5 – 2% . u_{pAl} was inferred from the measured flyer velocity and an impedance matching method, using the known Hugoniot response of aluminum and titanium. Thus, the uncertainty in u_{pAl} had contributions from both the uncertainty in the measured flyer velocity (typically ~ 0.5 – 1%) and the uncertainty associated with the impedance matching process.

For experiments using aluminum flyer plates, the impacts were nearly symmetric (slightly different densities due to shock formation in the flyer plate, and due to cryogenic temperature of the drive plate). In these cases the particle velocity could be determined to within ~ 0.5 – 1% , from the measured flyer plate velocities and slight corrections to the expression $u_{pAl} = u_v/2$ expected for purely symmetric impacts (see Ref. 41 for details). For purposes of uncertainty analysis, a value of 1% , which represents an upper bound, was taken to be the contribution to the uncertainty due to the impedance matching process for experiments using aluminum flyer plates. To be conservative, $\delta u_{pAl}/u_{pAl}$ for the aluminum flyer plate experiments was taken as the linear sum of the uncertainty in the measured flyer velocity (typically ~ 0.5 – 1%) and the 1% uncertainty due to impedance matching, as opposed to the square root of the quadratic sum.

For experiments using titanium flyer plates, which are clearly nonsymmetric impact conditions, the uncertainty in the high-stress EOS of both aluminum and titanium must be taken into account. For this discussion it is assumed that the U_s - u_p response of both materials can be treated as linear (i.e., $U_s = C + S u_p$) in the stress range of interest (~ 200 – 700 GPa). Given this assumption, and the Rankine Hugoniot conservation equations,⁵³ the stress state of the target material and flyer plate material can be written as

$$\begin{aligned}
 \sigma &= \rho_{al}(C_{al} + S_{al}u_{pAl})u_{pAl} \\
 &= \rho_{ti}\{C_{ti} + S_{ti}(u_v - u_{pAl})\}(u_v - u_{pAl}), \quad (A1)
 \end{aligned}$$

where ρ_{al} and ρ_{ti} are the initial densities of the aluminum drive plate and titanium flyer plate, respectively, and C_{al} , S_{al} , C_{ti} , and S_{ti} are the coefficients of the linear U_s - u_p relations for aluminum and titanium. Equation (A1) can be solved for u_{pAl} :

$$u_{pAl} = \frac{\sqrt{\left(\frac{\rho_{al}}{\rho_{ti}}C_{al} + C_{ti} + 2S_{ti}u_v\right)^2 + 4u_v\left(\frac{\rho_{al}}{\rho_{ti}}S_{al} - S_{ti}\right)(C_{ti} + S_{ti}u_v) - \left(\frac{\rho_{al}}{\rho_{ti}}C_{al} + C_{ti} + 2S_{ti}u_v\right)}}{2\left(\frac{\rho_{al}}{\rho_{ti}}S_{al} - S_{ti}\right)}. \quad (\text{A2})$$

Following standard techniques for uncertainty analysis,⁵¹ uncertainties in u_{pAl} due to uncertainties in C_{al} , S_{al} , C_{ti} , and S_{ti} would be determined by evaluating partial derivatives of Eq. (A2) with respect to these variables. However, these partial derivatives are quite involved and are omitted here. Instead, variations in u_{pAl} were evaluated for reasonable changes in each of C_{al} , S_{al} , C_{ti} , and S_{ti} , within the bounds of the experimental data for aluminum and titanium.^{41,78–80} For reasonable uncertainties in C_{al} , S_{al} , C_{ti} , and S_{ti} ($\sim 2\text{--}3\%$ and $\sim 5\%$ for the aluminum and titanium coefficients, respectively), the resulting variations in u_{pAl} obtained from Eq. (A2) were of order $\pm 0.2\text{--}1\%$, with the largest variation due to the uncertainty in S_{ti} . The total uncertainty in u_{pAl} due to the impedance matching process was then taken to be the square root of the quadratic sum of these variations in u_{pAl} . For purposes of uncertainty analysis, a value of 2%, which corresponds to a 1% variation resulting from variations in each C_{al} , S_{al} , C_{ti} , and S_{ti} , was taken to be the contribution to the uncertainty due to the impedance matching process for experiments using titanium flyer plates. To be conservative, $\delta u_{pAl}/u_{pAl}$ for the titanium flyer plate experiments was taken as the linear sum of the uncertainty in the measured flyer velocity (typically $\sim 0.5\text{--}1\%$) and the 2% uncertainty due to impedance matching, as opposed to the square root of the quadratic sum.

Given U_s and u_{pAl} , the following procedure was followed to determine u_p , P , ρ_1/ρ_0 , and the associated uncertainties. The Sesame 3700 EOS model⁵⁴ was used to calculate the release isentrope from the shock state of the aluminum drive plate defined by u_{pAl} . Two pressure-particle velocity points (P_1, u_{p1}) and (P_2, u_{p2}) were chosen along the release isentrope in the vicinity of the LD_2 Hugoniot point; one point a few GPa above and one point a few GPa below the chord defined by $\rho_0 U_s$. These points were used to determine the approximate slope S of the release isentrope in the vicinity of the LD_2 Hugoniot point, i.e.,

$$S \equiv \frac{P_1 - P_2}{u_{p1} - u_{p2}}. \quad (\text{A3})$$

u_p , P , and ρ_1/ρ_0 could then be determined from the intersection of the straight line through the point (P_1, u_{p1}) with slope S and the chord defined by $\rho_0 U_s$:

$$u_p = \frac{P_1 - S u_{p1}}{\rho_0 U_s - S}, \quad (\text{A4})$$

$$P = \rho_0 U_s \left(\frac{P_1 - S u_{p1}}{\rho_0 U_s - S} \right), \quad (\text{A5})$$

and

$$\frac{\rho_1}{\rho_0} = \frac{U_s(\rho_0 U_s - S)}{U_s(\rho_0 U_s - S) - (P_1 - S u_{p1})}. \quad (\text{A6})$$

Equations (A4)–(A6) depend on the quantities P_1 , u_{p1} , and S which relate to the release isentrope. As mentioned above, in this analysis we treat the release response of aluminum as being known. However, there remains an uncertainty in the location of the release isentrope due to the uncertainty in the shock state of the aluminum drive plate. It is expected that variations in S are small for slightly different initial shock states in the drive plate, and thus are neglected. The remaining uncertainty in the location of the release isentrope is effectively an uncertainty in the point (P_1, u_{p1}). Since the release isentrope is being treated as a straight line of slope S , the uncertainty in both P_1 and u_{p1} can be reduced to an effective uncertainty in one of the two variables; the uncertainty in P_1 can be accounted for by an equivalent, additional uncertainty in u_{p1} .⁵¹ Comparison of release isentropes spanning the initial shock states in the drive plate given by $u_{pAl} \pm \delta u_{pAl}$, where δu_{pAl} was determined as described above, indicates that for a given P_1 the variation in u_{p1} is such that

$$\frac{\delta u_{p1}}{u_{p1}} \approx \frac{\delta u_{pAl}}{u_{pAl}}, \quad (\text{A7})$$

at least in the pressure range of interest for this study. Therefore the fractional uncertainty in u_{p1} was taken to be equal to the fractional uncertainty in u_{pAl} .

Following standard techniques for uncertainty analysis,⁵¹ uncertainties in u_p , P , and ρ_1/ρ_0 due to uncertainties in U_s and u_{p1} were then determined through the following relations:

$$\delta u_p = \sqrt{\left(\frac{\partial u_p}{\partial u_{p1}} \delta u_{p1}\right)^2 + \left(\frac{\partial u_p}{\partial U_s} \delta U_s\right)^2}, \quad (\text{A8})$$

$$\delta P = \sqrt{\left(\frac{\partial P}{\partial u_{p1}} \delta u_{p1}\right)^2 + \left(\frac{\partial P}{\partial U_s} \delta U_s\right)^2}, \quad (\text{A9})$$

and

$$\delta \frac{\rho_1}{\rho_0} = \sqrt{\left(\frac{\partial \rho_1/\rho_0}{\partial u_{p1}} \delta u_{p1}\right)^2 + \left(\frac{\partial \rho_1/\rho_0}{\partial U_s} \delta U_s\right)^2}, \quad (\text{A10})$$

where u_p , P , and ρ_1/ρ_0 are given by Eqs. (A4)–(A6). These are the values of the uncertainties listed in Table I.

We reiterate that the above discussion is concerned with the random errors associated with measurement of the shocked state of the drive plate and the LD_2 shock velocity,

assuming that the release response of aluminum is adequately described by the Sesame 3700 model. We acknowledge that there is the possibility of a systematic error associated with the aluminum release response. However, based on the aluminum release measurements using silica aerogel (described in Sec. V) and the internal self-consistency of the three measurements performed in this study (described in

Sec. IV), we feel that this potential systematic error, if present, must be small. The effect of the systematic error would be slight shifts in the inferred density compression, of order a few percent. Since the shift would be nominally the same amount for each data point we deem it appropriate to treat this potential source of error separately from the discussion of the random errors given above.

- *Present address: Institute for Shock Physics and Department of Physics, Washington State University, Pullman, Washington 99164-2816.
- ¹L.B. Da Silva, P. Celliers, G.W. Collins, K.S. Budil, N.C. Holmes, T.W. Barbee, Jr., B.A. Hammel, J.D. Kilkenny, R.J. Wallace, M. Ross, R. Cauble, A. Ng, and G. Chiu, *Phys. Rev. Lett.* **78**, 483 (1997).
 - ²G.W. Collins, L.B. Da Silva, P. Celliers, D.M. Gold, M.E. Foord, R.J. Wallace, A. Ng, S.V. Weber, K.S. Budil, and R. Cauble, *Science* **281**, 1178 (1998).
 - ³G.I. Kerley, *Phys. Earth Planet. Inter.* **6**, 78 (1972); G.I. Kerley (unpublished).
 - ⁴M. Ross, F.H. Ree, and D.A. Young, *J. Chem. Phys.* **79**, 1487 (1983).
 - ⁵D.A. Young and E.M. Corey, *J. Appl. Phys.* **78**, 3748 (1995).
 - ⁶A.N. Mostovych, Y. Chan, T. Lehecha, A. Schmitt, and J.D. Sethian, *Phys. Rev. Lett.* **85**, 3870 (2000).
 - ⁷A.N. Mostovych, Y. Chan, T. Lehecha, L. Phillips, A. Schmitt, and J.D. Sethian, *Phys. Plasmas* **8**, 2281 (2001).
 - ⁸M.D. Knudson, D.L. Hanson, J.E. Bailey, C.A. Hall, J.R. Asay, and W.W. Anderson, *Phys. Rev. Lett.* **87**, 225501 (2001).
 - ⁹M.D. Knudson, D.L. Hanson, J.E. Bailey, C.A. Hall, and J.R. Asay, *Phys. Rev. Lett.* **90**, 035505 (2003).
 - ¹⁰S.I. Belov, G.V. Boriskov, A.I. Bykov, R.I. Il'kaev, N.B. Luk'yanov, A.Ya. Matveev, O.L. Mikhailova, V.D. Selemir, G.V. Simakov, R.F. Trunin, I.P. Trusov, V.D. Urlin, V.E. Fortov, and A.N. Shuikin, *Pis'ma Zh. Eksp. Teor. Fiz.* **76**, 508 (2002) [*JETP Lett.* **76**, 433 (2002)].
 - ¹¹G.V. Boriskov, A.I. Bykov, R.I. Il'kaev, V.D. Selemir, G.V. Simakov, R.F. Trunin, V.D. Urlin, V.E. Fortov, and A.N. Shuikin, *Dokl. Akad. Nauk* **392**, 755 (2003) [*Dokl. Phys.* **48**, 553 (2003)].
 - ¹²R.F. Trunin and W.J. Nellis (unpublished).
 - ¹³T.R. Boehly, D.G. Hicks, P.M. Celliers, T.J.B. Collins, J.H. Eggert, S.J. Moon, E. Vianello, D.D. Meyerhofer, and G.W. Collins (private communication).
 - ¹⁴W.J. Nellis, *Phys. Rev. Lett.* **89**, 165502 (2002).
 - ¹⁵W.R. Magro, D.M. Ceperley, C. Pierleoni, and B. Bernu, *Phys. Rev. Lett.* **76**, 1240 (1996).
 - ¹⁶B. Militzer and D.M. Ceperley, *Phys. Rev. Lett.* **85**, 1890 (2000).
 - ¹⁷I. Kwon, J.D. Kress, and L.A. Collins, *Phys. Rev. B* **50**, 9118 (1994).
 - ¹⁸L. Collins, I. Kwon, J. Kress, N. Troullier, and D. Lynch, *Phys. Rev. E* **52**, 6202 (1995).
 - ¹⁹T.J. Lenosky, J.D. Kress, and L.A. Collins, *Phys. Rev. B* **56**, 5164 (1997).
 - ²⁰T.J. Lenosky, S.R. Bickham, J.D. Kress, and L.A. Collins, *Phys. Rev. B* **61**, 1 (2000).
 - ²¹G. Galli, R.Q. Hood, A.U. Hazi, and F. Gygi, *Phys. Rev. B* **61**, 909 (2000).
 - ²²S. Bagnier, P. Blottiau, and J. Clerouin, *Phys. Rev. E* **63**, 015301(R) (2001).
 - ²³M.P. Desjarlais, *Phys. Rev. B* **68**, 064204 (2003).
 - ²⁴F. Gygi and G. Galli, *Phys. Rev. B* **65**, 220102(R) (2002).
 - ²⁵M. Ross, *Phys. Rev. B* **54**, R9589 (1996).
 - ²⁶D. Saumon, W.B. Hubbard, A. Burrows, T. Guillot, J.I. Lunine, and G. Chabrier, *Astrophys. J.* **460**, 993 (1996).
 - ²⁷F.J. Rogers and D.A. Young, *Phys. Rev. E* **56**, 5876 (1997).
 - ²⁸M. Ross, *Phys. Rev. B* **58**, 669 (1998).
 - ²⁹M. Ross and L.H. Yang, *Phys. Rev. B* **64**, 134210 (2001).
 - ³⁰D.A. Young, *High Press. Res.* **16**, 389 (2000); (private communication).
 - ³¹R.D. Dick and G.I. Kerley, *J. Chem. Phys.* **73**, 5264 (1980).
 - ³²M. van Thiel, M. Ross, B.L. Hord, A.C. Mitchell, W.H. Gust, M.J. D'Addario, and R.N. Keeler, *Phys. Rev. Lett.* **31**, 979 (1973).
 - ³³M. van Thiel, L.B. Hord, W.H. Gust, A.C. Mitchell, M. D'Addario, K. Boutwell, E. Wilbarger, and B. Barrett, *Phys. Earth Planet. Inter.* **9**, 57 (1974).
 - ³⁴W.J. Nellis, A.C. Mitchell, M. van Thiel, G.J. Devine, R.J. Trainor, and N. Brown, *J. Chem. Phys.* **79**, 1480 (1983).
 - ³⁵We acknowledge that others have used reshock and reverberating shock techniques (see, for example, Refs. 31–34,36). However, in this context, these studies represent the use of these techniques to attempt to discern the limiting shock compression in this high pressure regime.
 - ³⁶W.J. Nellis, S.T. Weir, and A.C. Mitchell, *Phys. Rev. B* **59**, 3434 (1999).
 - ³⁷G.I. Kerley (unpublished).
 - ³⁸In previous publications (Refs. 8,9) we compared our experimental results with an earlier, incomplete revision of the Sesame 72 model, referred therein as the Sesame model (also known as the Sesame 98 or Kerley 98 model). The current revision, referred to as the Kerley 03 model, consists of several improvements over the earlier revision. At the request of the author of these models (G.I. Kerley), we have done away with the earlier revision of the Sesame 72 model in favor of the more recent revision.
 - ³⁹M.K. Matzen, *Phys. Plasmas* **4**, 1519 (1996).
 - ⁴⁰M.D. Knudson, D.L. Hanson, J.E. Bailey, C.A. Hall, J.R. Asay, and C. Deeney (unpublished).
 - ⁴¹M.D. Knudson, R.W. Lemke, D.B. Hayes, C.A. Hall, C. Deeney, and J.R. Asay, *J. Appl. Phys.* **94**, 4420 (2003).
 - ⁴²R.W. Lemke, M.D. Knudson, C.A. Hall, T.A. Hail, P.M. Desjarlais, J.R. Asay, and T.A. Mehlhorn, *Phys. Plasmas* **10**, 1092 (2003).
 - ⁴³R.W. Lemke, M.D. Knudson, A.C. Robinson, T.A. Hail, K.W. Struve, J.R. Asay, and T.A. Mehlhorn, *Phys. Plasmas* **10**, 1867 (2003).
 - ⁴⁴D.L. Hanson, J.R. Asay, C.A. Hall, M.D. Knudson, J.E. Bailey, K.J. Fleming, R.R. Johnston, B.F. Clark, M.A. Bernard, W.W.

- Anderson, G. Hassall, and S.D. Rothman, in *Shock Compression of Condensed Matter-1999*, edited by M.D. Furnish, L.C. Chhabildas, and R.S. Hixson (AIP Press, New York, 2000), p.1175; D.L. Hanson, R.R. Johnston, M.D. Knudson, J.R. Asay, C.A. Hall, J.E. Bailey, and R.J. Hickman, in *Shock Compression of Condensed Matter-2001*, edited by M.D. Furnish, N.N. Thadani, and Y. Horie (AIP Press, New York, 2002), p. 1141.
- ⁴⁵Y.S. Touloukian, R.K. Kirby, R.E. Taylor, P.D. Desai, *Thermal Expansion—Metallic Elements and Alloys*, Vol. 12 of *Thermophysical Properties of Matter* (IFI/Plenum, New York, 1975), pp. 2, 77.
- ⁴⁶Y.S. Touloukian, R.K. Kirby, R.E. Taylor, and T.Y.R. Lee, *Thermal Expansion—Nonmetallic Solids*, Vol. 13 of *Thermophysical Properties of Matter* (IFI/Plenum, New York, 1977), pp. 176, 350.
- ⁴⁷For example, the linear correction $(L_2-L_1)/L_1$ for Cu at 20 K is $-0.324 (\pm 0.010)\%$ or $-2.6 (\pm 0.1) \mu\text{m}$ for an $800 \mu\text{m}$ thick reference spacer. The largest thermal expansion correction for any material was that for aluminum, $-0.415 (\pm 0.01)\%$ at 20 K.
- ⁴⁸The initial flyer thickness was nominally $800 \mu\text{m}$. The $\sim 300 \mu\text{m}$ thickness refers to portion of the flyer at impact that remained unaffected by magnetic diffusion.
- ⁴⁹L.M. Barker and R.E. Hollenbach, *J. Appl. Phys.* **43**, 4669 (1972).
- ⁵⁰The VISAR, FOSBO, and self-emission records shown in Fig. 2, which have been time shifted to align the shock break out of each diagnostic at the aluminum/ LD_2 interface, appear to exhibit dissimilar rise times. This is a result of the different time resolutions for each of the diagnostics. In this case (Z824S), the time resolutions of the diagnostics were $\sim 1-2$, ~ 1 , and ~ 0.5 ns for the VISAR, FOSBO, and self-emission, respectively.
- ⁵¹J.R. Taylor, *An Introduction to Error Analysis*, 2nd ed. (University Science Books, California, 1982), p. 184.
- ⁵²Greg Dunham, J.E. Bailey, A. Carlson, P. Lake, and M.D. Knudson, *Rev. Sci. Instrum.* **75**, 928 (2004).
- ⁵³G.E. Duvall and R.A. Graham, *Rev. Mod. Phys.* **49**, 523 (1977).
- ⁵⁴G.I. Kerley, *Int. J. Impact Eng.* **5**, 441 (1987); G.I. Kerley (unpublished).
- ⁵⁵G.I. Kerley (unpublished).
- ⁵⁶The flyer plate experiences further quasi-isentropic compression and release, but since that process is reversible we only need consider the release from the shocked state. Also, the density, temperature, and particle velocity of the flyer at impact are not constants. Since the shock forms at the foot of the pulse and grows with distance, the density is lower and the temperature is higher towards the impact side of the flyer plate. However, given that we are only concerned with approximately $200-300 \mu\text{m}$ of the impact side of the flyer and the low rate of shock growth, the magnitude of the gradients are not significant, and can be ignored.
- ⁵⁷The assertion that $\rho_2 \approx 1.9\rho_1$ is also supported by the reshock experiments described in Sec. III B. The data listed in Tables II and III indicate that for sapphire anvils ρ_2 was experimentally observed to be $\sim 1.96\rho_1$, on average.
- ⁵⁸The collection fiber used in the FOSBO measurement collected self-emission from the shock-heated LD_2 in addition to the reflected laser light. A portion of this self-emission signal was transmitted through the band-pass filter used in the FOSBO diagnostic, thus providing a measure of the self-emission in accordance with that obtained by the spectroscopy diagnostic.
- ⁵⁹The emission observed after the shock reflected from the LD_2 /sapphire interface is in good agreement with the expected reshock temperature of LD_2 ($\sim 1-2$ eV), and much greater than the shocked sapphire temperature (few tenths of an eV).
- ⁶⁰J.M. McGlaun, S.L. Thompson, and M.G. Elrick, *Int. J. Impact Eng.* **10**, 351 (1990).
- ⁶¹The first and second shock in the anvil (sapphire or α -quartz) were at pressure levels of $\sim 300-400$ GPa and $\sim 600-800$ GPa, respectively, corresponding the shock temperatures of $\sim 0.5-0.75$ eV and $\sim 1-2$ eV, respectively. The observed increase in emission corresponded to the resulting temperature increase as the second shock overtook the first shock.
- ⁶²The Kerley 03 model was used to look at the effect of the slightly different initial density in the present study. Hugoniot for initial densities of 0.17 and 0.167 g/cm^3 were computed and plotted as pressure vs density compression. The Hugoniot for 0.167 g/cm^3 was found to be about 0.7% higher in compression, i.e., softer, than that for 0.17 g/cm^3 .
- ⁶³B.L. Glushak, A.P. Zharkov, M.V. Zhernokletov, V.Ya. Ternovoi, A.S. Filimonov, and V.E. Fortov, *Zh. Eksp. Teor. Fiz.* **96**, 1301 (1989) [*Sov. Phys. JETP* **69**, 739 (1989)].
- ⁶⁴Based on the Kerley 03 EOS model, the density compressions at 60 and 120 GPa are 4.01 and 3.99, respectively, for initially solid samples (0.199 g/cm^3). This compares to 4.26 and 4.15, respectively, for initially liquid samples (0.17 g/cm^3).
- ⁶⁵S.P. Lyon and J.D. Johnson (unpublished).
- ⁶⁶B. Militzer, D.M. Ceperley, J.D. Kress, J.D. Johnson, L.A. Collins, and S. Mazevet, *Phys. Rev. Lett.* **87**, 275502 (2001).
- ⁶⁷M.P. Desjarlais (private communication).
- ⁶⁸G.I. Kerley (unpublished).
- ⁶⁹M. Ross and L.H. Yang, *Phys. Rev. B* **64**, 174102 (2001).
- ⁷⁰N.C. Holmes, in *High-Pressure Science and Technology-1993*, edited by S.C. Schmidt, J.W. Shaner, G.A. Samara, and M. Ross (AIP Press, New York, 1994), p. 153.
- ⁷¹The power varies as a function of wavelength; at 400 and 600 nm the power is approximately 1.9 and 1.5, respectively.
- ⁷²K.S. Holian (unpublished).
- ⁷³S.P. Lyon and J.D. Johnson (unpublished).
- ⁷⁴S.L. Thompson (unpublished).
- ⁷⁵K.S. Trainor (unpublished).
- ⁷⁶R.F. Trunin, in *Shock Compression of Condensed Materials* (University Press, Cambridge, 1998).
- ⁷⁷D.M. Hicks, P.M. Celliers, G.W. Collins, J.H. Eggert, and S.J. Moon, *Phys. Rev. Lett.* **91**, 035502 (2003).
- ⁷⁸N.A. Winfree, L.C. Chhabildas, W.D. Reinhart, D.E. Carroll, and G.I. Kerley, in *Shock Compression of Condensed Matter-2001*, edited by M.D. Furnish, N.N. Thadani, and Y. Horie (AIP Press, New York, 2002), p. 75.
- ⁷⁹L.V. Al'tshuler, A.A. Bakanova, I.P. Dudoladov, E.A. Dynin, R.F. Trunin, and B.S. Chekin, *Zh. Prikl. Mekh. Tekhn. Fiz.* **2**, 3 (1981) [*J. Appl. Mech. Tech. Phys.* **22**, 145 (1981)].
- ⁸⁰R.F. Trunin, N.V. Panov, and A.B. Medvedev, *Pis'ma Zh. Eksp. Teor. Fiz.* **62**, 572 (1995) [*JETP Lett.* **62**, 591 (1995)].